

Advanced Electrochemical Analysis for Energy Storage Interfaces

Jingshu Hui,[‡] Zachary T. Gossage,[‡] Dipobrato Sarbapalli,[§] Kenneth Hernández-Burgos,^{‡,¶} and Joaquín Rodríguez-López*,^{‡,¶}

■ CONTENTS	
Classical Electrochemistry for Materials Analysis	61
Cyclic Voltammetry	62
Galvanostatic Charge—Discharge	63
Electrochemical Impedance Spectroscopy	63
Electrochemical Quartz Crystal Microbalance	63
Potentiostatic and Galvanostatic Intermittent	
Titration Techniques	64
Advanced Electrochemical Scanning Probe Micros-	
сору	65
Scanning Electrochemical Microscopy	65
SECM Operation Modes	66
Redox Reactivity	66
Mapping Ionic Processes	67
Limitations and Future Directions	67
Scanning Ion Conductance Microscopy	68
Topography and Ionic Conductance Detection	68
Limitations and Future Direction	69
Scanning Micropipette Contact Method	69
Scanning Electrochemical Cell Microscopy	70
Advantages and Limitations	70
Other Electrochemical Coupled Scanning Probe	
Microscopy	70
In Situ AFM for LIB Anode	70
In Situ AFM for LIB Cathodes	71
In Situ AFM Beyond LIBs	71
Future Directions	71
Electrochemical Coupled In Situ Characterization	72
Fourier Transform Infrared Spectroscopy	72
Evaluation of the SEI	73
Application for Beyond LIBs	73
Limitations and Future Directions	74
Raman Spectroscopy	74
Surface-Enhanced Raman Spectroscopy	74
Limitation and Future Directions	74
Sum Frequency Generation Spectroscopy	74
Tracking Molecular Orientation and Break-	
down	74
Advantages and Limitations	76
X-ray Absorption Spectroscopy	76
Surface Structure and Speciation Analysis	76
Limitations and Future Directions	76 76
X-ray Photoelectron Spectroscopy	76 76
Oxidation State and Species Identification Current Limitations	76 77
Current Limitations	//

X-ray Reflectometry	77
Neutron Reflectometry	77
Transmission Electron Microscopy	77
Solid-Liquid Interface	77
Solid-Solid Interface	78
Current Limitations	78
Final Remarks	78
Author Information	79
Corresponding Author	79
ORCID	79
Notes	79
Biographies	79
Acknowledgments	79
References	79

ne of Wolfgang Pauli's, 1945 Nobel Prize in Physics, most popular quotes reads "God made the bulk; the surface was invented by the devil." When it comes to energy storage, interfaces, structures created between dissimilar media, such as liquids and solids, and interphases, structures arising in between these dissimilar media, inherit this notorious reputation. This is because the high-energy density chemical systems comprising the most attractive energy storage technologies are host to a plethora of dynamic processes, 2 including electron transfer, ion transfer and migration, nucleation and dissolution, side reactions, and solvation/desolvation processes, to name a few, that significantly alter their landscape. This presents a fascinating challenge to the analysis of the interfacial region, increasing its complexity from a problem of surface sensitivity to one of transient, electrochemically-driven behavior and requiring measurement across scales and through materials. It is precisely these demanding characteristics that have made the creation of analytical tools and methods a priority direction in the assessment of needs for energy storage.3

The great diversity of energy technologies spans multifarious phenomena involving chemical transformations, ion intercalation, adsorption, and metal plating, all of which enable the functioning of batteries and supercapacitors. Despite this diversity, the interface between the electrode and electrolyte is a common structure that plays an indispensable role for enabling

Special Issue: Fundamental and Applied Reviews in Analytical Chemistry 2019

Published: November 14, 2018



[‡]Department of Chemistry, University of Illinois at Urbana-Champaign, 600 South Mathews Avenue, Urbana, Illinois 61801, United States

[§]Department of Materials Science and Engineering, University of Illinois at Urbana—Champaign, 1304 West Green Street, Urbana, Illinois 61801, United States

[¶]Beckman Institute for Advanced Science and Technology, 405 North Mathews Avenue, Urbana, Illinois 61801, United States

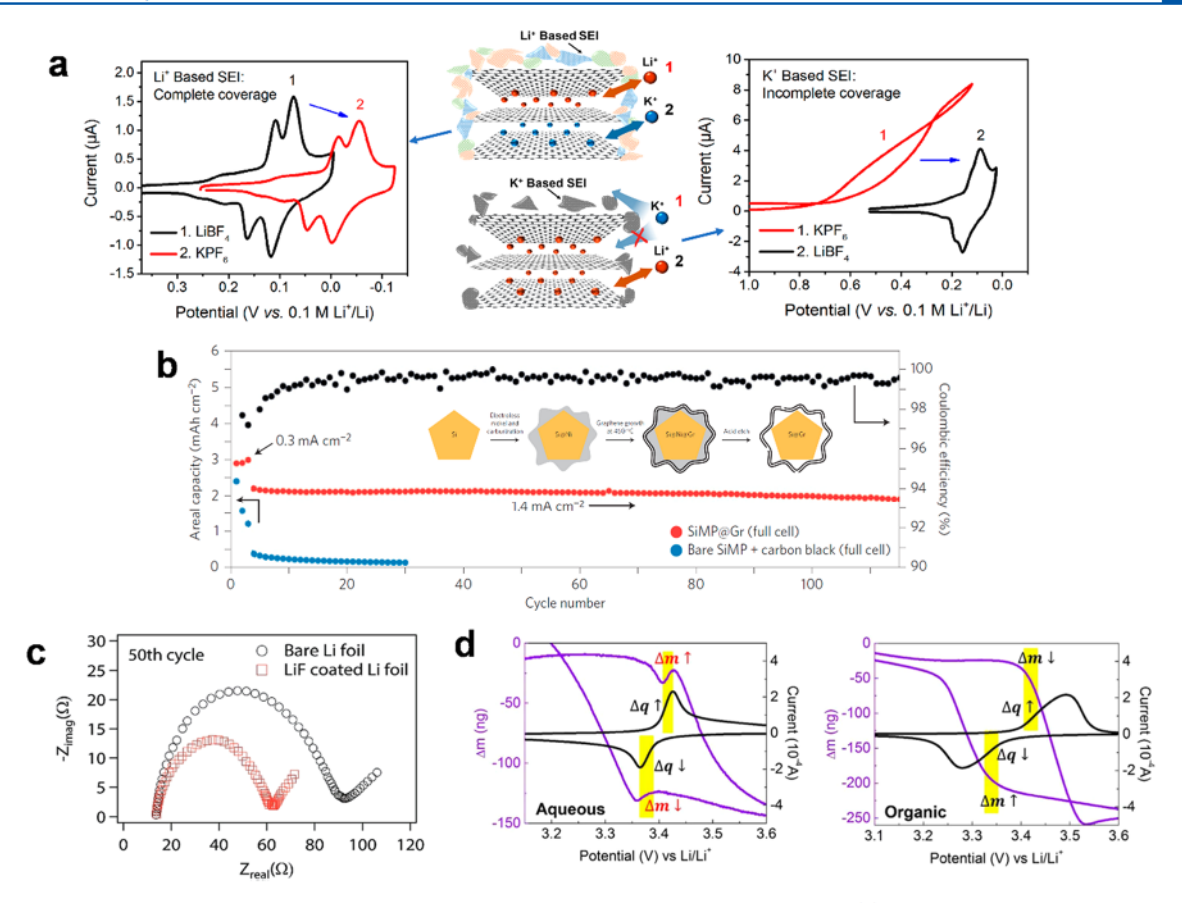


Figure 1. Classical electroanalytical methods for the investigation of emerging energy storage interfaces. (a) Study of the influence of SEI conditioning on alkali-ion intercalation explored via CV. K⁺ intercalation is only achieved with the full passivation of Li⁺-based SEI, whereas a K⁺-based SEI leads to irreversible deposition. (b) Conformal coating of graphene around Si nanoparticles leads to high cycling life and efficiency compared to bare Si nanoparticles, as observed through galvanostatic cycling. (c) LiF coating on Li metal decreased charge transfer resistance, as observed through EIS. (d) EQCM shows deviation from monotonic mass loss upon oxidation and vice versa upon reduction when LiFePO₄ was cycled in aqueous media (left). No such deviations from the expected behavior were observed when LiFePO₄ was cycled in organic media (right). Part (a) reproduced from Hui, J.; Schorr, N. B.; Pakhira, S.; Qu, Z.; Mendoza-Cortes, J. L.; Rodriguez-López, J. J. Am. Chem. Soc. 2018, 140, 13599–13603 (ref 23). Copyright 2018 American Chemical Society. Part (b) reprinted by permission from Macmillan Publishers Ltd.: Nature Energy, Li, Y.; Yan, K.; Lee, H.-W.; Lu, Z.; Liu, N.; Cui, Y. Nat. Energy 2016, 1, 15029 (ref 27). Copyright 2016. Part (c) reproduced from Fan, L.; Zhuang, H. L.; Gao, L.; Lu, Y.; Archer, L. A. J. Mater. Chem. A 2017, 5, 3483–3492 (ref 28), with permission of The Royal Society of Chemistry. Part (d) reprinted from Song, X.; Liu, T.; Amine, J.; Duan, Y.; Zheng, J.; Lin, Y.; Pan, F. Nano Energy 2017, 37, 90–97 (ref 29). Copyright 2017, with permission from Elsevier.

efficient electronic and ionic mobility. Therefore, fundamental studies at both model systems and at real devices are desirable and complementary. For an operating energy storage system, it is important to keep a balance between dimension, morphology, porosity, tortuosity, and chemically specific electronic interactions at the dominating interfaces. Ion diffusion/intercalation and reactivity mechanisms in solid-state materials are often multistep and rely on the structure, overpotential, and any modification at the material surface. With these characteristics in mind, it is important to highlight the value of new electroanalytical approaches designed to study fluxes of electrons and ions, reactivity, and structural changes and heterogeneity at operating interfaces. All these directions constitute the main focus points of this Review.

We will discuss three major categories of electrochemical techniques: classical electrochemical methods, advanced scanning probe microscopy, and multimodal characterization techniques. Classical amperometric and potentiometric electrochemical analyses provide indirect information on the electrode materials' response toward external changes of solvent, electrolyte, and surface modification. Combining these techniques with electrochemistry-based scanning probe microscopy, spectros-

copy, X-ray, and electron microscopy provides a powerful method for understanding the interfacial chemistry on an in situ platform. For example, electrochemical imaging gives unprecedented insights into the distribution of site reactivity that leads to the observed macroscopic performance of electrode interfaces. In addition, electronic probes obtain local redox activity, electronic conductivity, and ionic permeability of the energy storage interface, while in situ spectroscopic techniques can acquire molecular- and atomic-level information. The progress in analytical techniques for bulk electrode materials and electrolyte assessment is summarized in previously published reviews.^{2,7–10} Numerous works related to interfacial structure, components, and reactivity of battery and supercapacitor systems were published in the last two years. This Review highly focuses on the recent developments between the years 2016-2018.

CLASSICAL ELECTROCHEMISTRY FOR MATERIALS ANALYSIS

Electrochemical techniques, including cyclic voltammetry (CV), ¹¹ galvanostatic charge—discharge, electrochemical impedance spectroscopy (EIS), ¹² potentiostatic intermittent

titration technique (PITT), galvanostatic intermittent titration technique (GITT), ¹³ and electrochemical quartz crystal microbalance (EQCM), ¹⁴ are the most widely used methods for energy related applications. These techniques are typically used directly on the bulk energy storage materials to obtain information about their charge storage mechanisms, charge diffusion, capacity, cyclability, and stability. ¹⁵ In this Review, we focused on pertinent works of interfaces in electrochemical energy storage.

Cyclic Voltammetry. CV provides information about the current—time—potential behavior of the electrode—electrolyte system under consideration and, therefore, is an extremely versatile electroanalytical technique. Typical CV responses depend on the ability of a species to exchange charge at the electrode—electrolyte interface. By adding specific redox mediators as probes, the interfacial properties of energy storage systems can be analyzed. CV has been used to understand and characterize the solid-electrolyte interphase (SEI) related surface deposition processes and interfacial activities, 21–23 as well as electron, ion, and molecule transport properties across interfaces. 24–26

SEI formation consists of an irreversible deposition process of solvent and electrolyte decomposition products that occur at negatively biased electrode surfaces. 30 The voltage and stability in which the SEI forms highly depend on the choice of solvent, scan rate,³¹ and electrolyte concentration.³² SEI formation in alloy-based anodes has been demonstrated to have a crystal orientation-controlled behavior.²⁰ The use of coupled techniques such as FT-IR and contact angle measurements with CV increased our knowledge of SEI formation across different Si crystal faces and different electrolytes. For example, an electrolyte decomposition product (LiF) was observed to be present in lesser quantities on the 110 face, when compared to the other crystalline faces. A similar study was performed at the Si (100) surface by Haregewoin et al., where they found the coverage of a 25 nm-thick binder has a selective influence of solvent transport properties, which alters the interfacial process formed at the Si surface.³³ CV was also used to probe the electrochemical accessibility of surface-modified electrodes. Nicolau et al. demonstrated that alkylphosphonic acid selfassembled monolayers (SAMs) controlled the wettability of solvent at the LiMn₂O₄ cathode surface, which influenced the molecule and ion mobility at the vicinity of the electrode.²⁴ This SAMs modification also helped prevent Mn²⁺ leaching from the

CV characterization of ultrathin electrodes provides direct information about interfacial processes and mechanisms. Unlike Li⁺ intercalation in bulk graphite material, 34 Hui et al. identified that the limited number of graphene sheets resulted in a lower order of intercalation stages. In another study of a similar few layer graphene (FLG) system, Hui et al. demonstrated that, by conditioning the interface of the graphitic material with a Li⁺containing SEI, reversible K+ intercalation was obtained at scan rates of up to 100 mV s⁻¹. The improved ion intercalation kinetics allowed CV exploration at scan rates at least three orders larger than anything reported for K⁺ intercalation.²³ As shown in the CV data in Figure 1a, the well-defined K⁺ staging peaks can only be obtained in the presence of a Li-based SEI. The usefulness of CV is that it clearly distinguishes the well-defined staging peaks from the irreversible deposition of K+-based inactive SEI (Figure 1a). This work highlights the importance of forming a suitable alkali-ion-based SEI for the intercalation of alkali metals. The micrometer-sized structure and ultrathin

thickness of FLG provides a network that allows fast charge/discharge processes, making this material an ideal platform for future alkali-ion storage studies. The restricted dimension facilitated ion diffusion approach is not unique to carbon-based material; Clancy and Rohan demonstrated a rapid CV cycling up to a scan rate of $100~\rm mV~s^{-1}$ at a binder free ultrathin LiCoO₂ film. ²⁵ A pseudocapacitive charge storage mechanism at fast scans was suggested, which might serve as new design principles for lithium-ion battery (LIB) electrodes with improved performance and rate capabilities.

CV provided a straightforward, yet powerful, characterization method for studies beyond ion intercalation at complex interfaces. Current-potential curves were used to study the effects of an interface consisting of a chemically deposited tin (Sn) layer on Li metal.³⁶ Derived from this data, a Tafel plot confirmed that the Sn coated Li-metal electrodes exhibited a lowered overpotential for Li plating/stripping compared to bare Li-metal electrodes. A similar approach was carried out by using an indium thin layer on a Li-metal substrate. 22 In this study, the CV showed that the indium was electrochemically active and participated in the charge/discharge process by forming an alloy with Li metal.²² In the case of magnesium batteries, CV was used to study the intercalation of MgCl⁺ into TiS₂ electrodes.²¹ The Randles-Sevcik analysis (i_{peak} vs the square root of scan rate) indicated a diffusion-limited intercalation process with no surface-limited adsorption.

CV analysis is useful at detecting the rate of soluble intermediates that are formed during electrolysis; these capabilities were used to inspect the reduction of S_8 to Li₂S, a complex process that is plagued by poor Coulombic efficiency and prolonged charging duration.³⁷ Lei et al. demonstrated that the surface modification of a carbon cloth electrode with TiO₂ nanowires substantially suppressed the shuttle effect (diffusion to the anode) of polysulfides and improved the capacity.¹⁸ The strong binding between TiO₂ "feathers" and LiS_x was identified as the main reason for restrained dissolution and diffusion of the soluble, reduced products. Wu et al. demonstrated a simple surface treatment method on Li metal by the addition of 250 ppm water to the electrolyte, which successfully prevented the shuttle effect.¹⁹ Here, a LiOH-rich SEI layer was proved to protect Li anode from reacting with polysulfides.

In summary, CV provides information about electrochemical systems in a rapid, reproducible, and efficient way. When coupled insightfully with electrode design, it can be a great ally to distinguish properties of interest. However, oftentimes, its use on bulk electrodes with the intention of selectively gaining information about the interface is limited. Another drawback of CV is that is relies on deriving diffusion coefficients through Randles-Sevcik relations. The diffusion of intercalating cations is well-known to depend on the state of the charge of the electrode and the interface composition.¹³ Therefore, the diffusivity cannot be represented by a single value for an electrochemical process. Despite these limitations, CV can be coupled with other characterization techniques to provide detailed, mechanistic descriptors of interfaces in the electrochemical system. Here, we will present several examples in the section titled Electrochemical Coupled In Situ Characterization, Limitations on the spatial resolution and surface sensitivity of electrochemical methods can also be accomplished through techniques like scanning probe microscopy, which will be discussed in later sections of Advanced Electrochemical Scanning Probe Microscopy.

Galvanostatic Charge-Discharge. Galvanostatic electrochemical methods involve passing a controlled current at the working electrode and measuring its potential response over time. 17 Galvanostatic cycling is a widely used method to quantify parameters of practical importance in energy storage systems, including the charge-discharge capacity, specific energy/power density, and cycle life of a specific material. 15,38 It also provides insights about mechanistic information such as intercalation staging, conversion reactions, and transport limitations of electrochemical processes via differential capacity curve analysis (i.e., $\delta Q/\delta V$ plots). Note that the studies involving galvanostatic charge-discharge are widespread throughout the research community, with around 2000 publications being listed for a search on Web of Science (Clarivate Analytics) using the keywords "Galvanostatic charge discharge" since 2016. Here, we only highlight several advancements and applications of these techniques for interface related studies.

Most of the interface related studies center around developing new electrode materials and tailoring interfaces for better performing energy storage systems.³⁹⁻⁴¹ As an emerging high capacity LIB anode, Si suffers from mechanical and interparticle connection failure due to large volume expansion (~300%) upon lithiation. 42 Encapsulation of Si in carbon-based structures has been an elegant solution to overcome the volumetric expansion. 43 For example, Li et al. suggested that, by using FLG cage encapsulation of Si nanoparticles (Figure 1b), the composite provided mechanical stability to the Si anodes during cycling with enhanced electrical connectivity.²⁷ Sun et al. explored the charge storage ability of packed thin graphite flakes architecture as a hybrid graphite-Li-metal anode. 44 An increased capacity of this artificial graphite microstructure beyond the theoretical intercalation limit of 372 mAh/g was observed. In addition to normal Li+ intercalation within graphite, the reversible entrapment of Li metal inside this microstructure was identified as the main reason for extra capacity gain. In all these studies, galvanostatic charge-discharge was used to prove that these materials with tailored interfaces show significant performance improvements over their original counterparts.

Galvanostatic methods have been used to understand the SEI related interfacial processes, including additive effects on SEI, 45,46 artificial SEI, 47-49 and protective coatings. 50 Dahn and co-workers demonstrated that Li₂FeO₂, when used as an additive, reduced the impedance across the SEI, which consequently decreased the tendency for pervasive side reactions. For example, undesirable Li plating can lead to dendrite formation and capacity losses in intercalation-type batteries. Therefore, galvanostatic cycling can indicate bulk improvements, such as the decrease in Li-plating, through discharge capacity measurements over time.⁵¹ The effectiveness of FLG as an artificial SEI on lithium nickel manganese cobalt oxide (LiNMC) cathodes was similarly evaluated by galvanostatic methods. The SEI was observed to improve capacity and rate capability during rapid cycling.⁵² The authors attributed these benefits to the ability of Li⁺ to migrate through defects in the stacked graphene interface. In addition, they suggested that the graphene coating preserved the local atomic structure of the active cathode materials during delithiation.

Similar to CV, galvanostatic charge—discharge methods provide indirect information about material cyclability upon interface modulation. Other characterizations using interfacesensitive techniques (such as synchrotron-based X-ray methods) are required to confirm these interfacial modifications.

More detailed studies can be found in the section Electrochemical Coupled In Situ Characterization.

Electrochemical Impedance Spectroscopy. Both CV and galvanostatic methods rely on the application of large potential perturbations to the electrochemical system (voltage or current) and then measurement of a transient response. Conversely, EIS involves applying a small alternating signal (typically the potential) to an electrochemical system at equilibrium. The ability of EIS to decouple ohmic polarization, charge transfer polarization (electron transfer kinetics), and concentration polarization (mass transfer kinetics) induced potential drops ¹⁶ can be used to directly quantify parameters of importance to energy storage systems such as charge transfer resistance, double layer capacitance, and diffusion coefficients. ⁵³

Several electrode architectures have been designed to address practical issues in batteries, such as capacity, cycling, and charge/discharge rates. 54-58 Many of these studies have utilized EIS measurements to directly characterize interface impedance. For example, the Li-metal anode prepared within a reduced graphene oxide scaffold was characterized through EIS. Dendrite formation led to increased charge transfer resistance in the case of plain Li foil electrodes, whereas the resistance to charge transfer was three times lower for Li-metal electrodes encapsulated in graphene oxide. Such measurements verified the stability of electrodes and enhanced Li plating/stripping kinetics. Similar effects were found on graphene-MnO electrodes. More examples of similar studies employing EIS can be found in the literature.

Multiple strategies have been proposed to stabilize the SEI on Li-metal anodes. ^{22,28,65} One approach involves the addition of In(TFSI)₃ to form an indium layer on Li-metal anodes. ²² EIS showed that the interfacial resistance decreased by an order of magnitude. EIS can also be combined with different theoretical models, such as DFT simulations. Recently, DFT and EIS were used to study artificial SEI layers, e.g., LiF on Li-metal anode ²⁸ (Figure 1c) and NaBr on Na metal anode. ⁶⁵ These artificial layers helped in reducing the diffusion barrier and improving stability. EIS measurements were compared with ex situ XPS at a graphite electrode, identifying a two-step mechanism behind the SEI formation. ⁶⁶ The approach uniquely assigned interface impedances measured through EIS to chemical species identified through XPS for the same state-of-charge.

In spite of its great prospects for decoupling bulk and interfacial processes, data analysis and interpretation for EIS measurements are challenging. The most common obstacle is to model an equivalent circuit with physical validity for the choice of elements (e.g., resistors, capacitors, Warburg impedances, among others). 15,53 Battery materials often involve a specialized electrode microstructure and heterogeneous interfaces (e.g., porous electrodes). These electrodes can involve multiple electrochemical charge transfer processes making the selection of a correct number of unknown elements in the equivalent circuit diagram difficult. Three-electrode setups and small electrode areas are preferred to reduce the difficulty factors of these measurements.¹⁵ Recent studies have also discussed typical circuit models for interpreting EIS data in batteries^{67,68} and the Warburg element in EIS model circuits, 69 both of which are key in the correct interpretation of EIS data.

Electrochemical Quartz Crystal Microbalance. The quartz crystal microbalance (QCM) is a highly sensitive gravimetric technique. The device detects changes in the resonance frequency of a quartz crystal by virtue of the deposition of small quantities of matter on itself. The decrease

in resonant frequency of the crystal is directly proportional to the thickness of the material deposited, which can be used to obtain its mass. This technique has been extended to electrochemical studies, known as EQCM, by utilizing a QCM crystal as the working electrode where electroactive films can be deposited on the crystal and mass changes in the film can be studied. 14 More details about the working principles of EQCM and its applicability in interfacial studies were described by Buttry and Ward in their review article. Some examples of EQCM applications described in their review include electrodeposition of metals, self-assembly of monolayers, and electrovalency measurements of anion adsorption. It should be noted that EQCM applications involve thin-film deposition, so interface effects dominate the EQCM response. Therefore, EQCM can be considered to provide direct information about interfaces in an electrochemical system.

With respect to energy storage materials, Song et al., ²⁹ have published a classical gravimetric EQCM study involving LiFePO₄ and NaFePO₄ materials cycled in organic and aqueous solvents. The EQCM response during oxidation (delithiation) was characterized by a monotonous decrease in mass and vice versa upon reduction (lithiation). However, this behavior was not observed in the case of LiFePO₄ when cycled in aqueous media, as shown in Figure 1d. This observation and subsequent DFT calculations revealed that the surface redox potential was approximately 0.5 V less than the bulk electrode, which led to readsorption of water during oxidation. Therefore, EQCM studies can be used in combination with other techniques to reveal useful mechanistic information about interfaces in electrochemical storage systems.

A recent development in EQCM is the use of in situ hydrodynamic spectroscopy. The technique has been utilized to study the structural changes at the mesoscale within thin-film battery electrodes.⁷³ The method successfully captured the magnitude of mesoscopic deformations in LiMn₂O₄ particles, and the results correlated well to measurements taken through a complementary in situ AFM measurement. In another study by Dargel et al., 74 two LiFePO₄ thin films were prepared on QCM sensors with small and large particle sizes, respectively. Smaller particles in a stiff binder experienced pure intercalation-based deformations. On the other hand, results with large particles indicated sliding friction and adhesion issues between the binder and active material. Other studies have utilized these hydrodynamic techniques 75,76 to characterize intercalation-induced gravimetric and viscoelastic changes in 2D Ti₃C₂(OH)₂ electrodes and to examine the influence of binder stiffness in the cycling performance of LiFePO₄ electrodes. The associated technicalities of in situ hydrodynamic spectroscopy have been reviewed previously.71,72

Another development in the field of EQCM is that of AC-electrogravimetry by Goubaa and co-workers. The technique involves coupling standard EQCM and EIS measurements. AC-electrogravimetry could differentiate and quantify ionic species adsorbed on the surface of reduced graphene oxide when tested in different aqueous electrolytes. It was revealed that the solvation of cations controlled the ease of adsorption into graphene oxide. This information was obtained because the mass of each species adsorbing could be distinguished by QCM, whereas EIS provided information about the kinetics of adsorption through which the identity of the species (ions, solvated ions, or water) was revealed. EQCM characterization can yield a wide variety of surface-specific information within electrochemical systems. However, the fundamentals behind the

topic are not straightforward, and many equations relevant to EQCM measurements are based on the assumption that changes of frequency translate into changes in mass; several other aspects are involved in deposition processes and thus more complex formulations are required. A detailed description of data analysis and common errors involved in EQCM experiments is presented in more detail in multiple review papers. 14,72

Potentiostatic and Galvanostatic Intermittent Titration Techniques. PITT⁷⁸ and GITT⁷⁹ are two powerful electroanalytical techniques developed in the late 1970s to measure the chemical diffusion coefficients within metallic alloy systems. Since their development, numerous studies have utilized these methods to characterize the solid-state diffusion of Li-ions into intercalation hosts. Recently, Levi and Aurbach¹³ have written a detailed review on the mathematical constructs behind both techniques and their comparison with EIS. In addition, they have reviewed several case studies utilizing EIS, PITT, and GITT to measure state-of-charge (SOC) dependent chemical diffusion coefficients of different electrode materials. Talaie et al., also described GITT methodology in a recent review.¹⁵

PITT and GITT experiments, as described by Levi and Aurbach, 13 involve the application of small increments of potential or current (respectively) so as to titrate a small quantity of charge at the electrode material. This incremental charge is measured and used in equations derived from Fickian diffusion relations, to yield the diffusion time constant $(\tau_{\rm d}).$ Combined with the characteristic diffusion length (L) of the electrode system, the chemical diffusion coefficient can be obtained by the relation $D_{\rm chem} = L^2/\tau_{\rm d}.$ This equation is valid for 1D diffusion and can be modified appropriately for different electrode systems.

PITT and GITT diffusion measurements are highly dependent on interfacial properties, and provide an indirect means to characterize them. Similar to other bulk methods (e.g. galvanostatic testing), the changes at the electrode interface or in its function lead to observable and quantifiable responses in the PITT and GITT analysis. For example, Yoo et al. 21 have modified TiS2 for Mg batteries in situ with an organic "pillar" compound, to increase the interlayer spacing. The resulting change in structure led to MgCl+ diffusion coefficients (measured through GITT) an order of magnitude higher than Mg²⁺ intercalation into MoS₂ and Mo₆S₈. A second study by Richard Prabakar et al.,80 involving graphene/CoSn(OH)6 composite electrodes, utilized PITT measurements to characterize the effect of graphene encapsulation of nanoparticulate CoSn(OH)6. PITT measurements indicated a significant increase in the diffusion coefficient of Li-ions into CoSn(OH)₆ upon encapsulation, which led the authors to believe that undesired structural changes in the active material were restricted by the graphene stacks.

Therefore, PITT and GITT experiments are excellent for quantifying chemical diffusion coefficients of Li-intercalation in solid-state electrodes. One advantage of utilizing PITT/GITT over EIS lies in the fact that EIS results have to be interpreted after constructing an equivalent circuit, which makes the data analysis difficult. On the other hand, PITT/GITT does not provide any other information different from diffusion coefficients, unlike EIS which provides several parameters directly related to the interface. Also, PITT/GITT does not provide direct information about interfaces, and the time for such experiments can span over days. ¹³

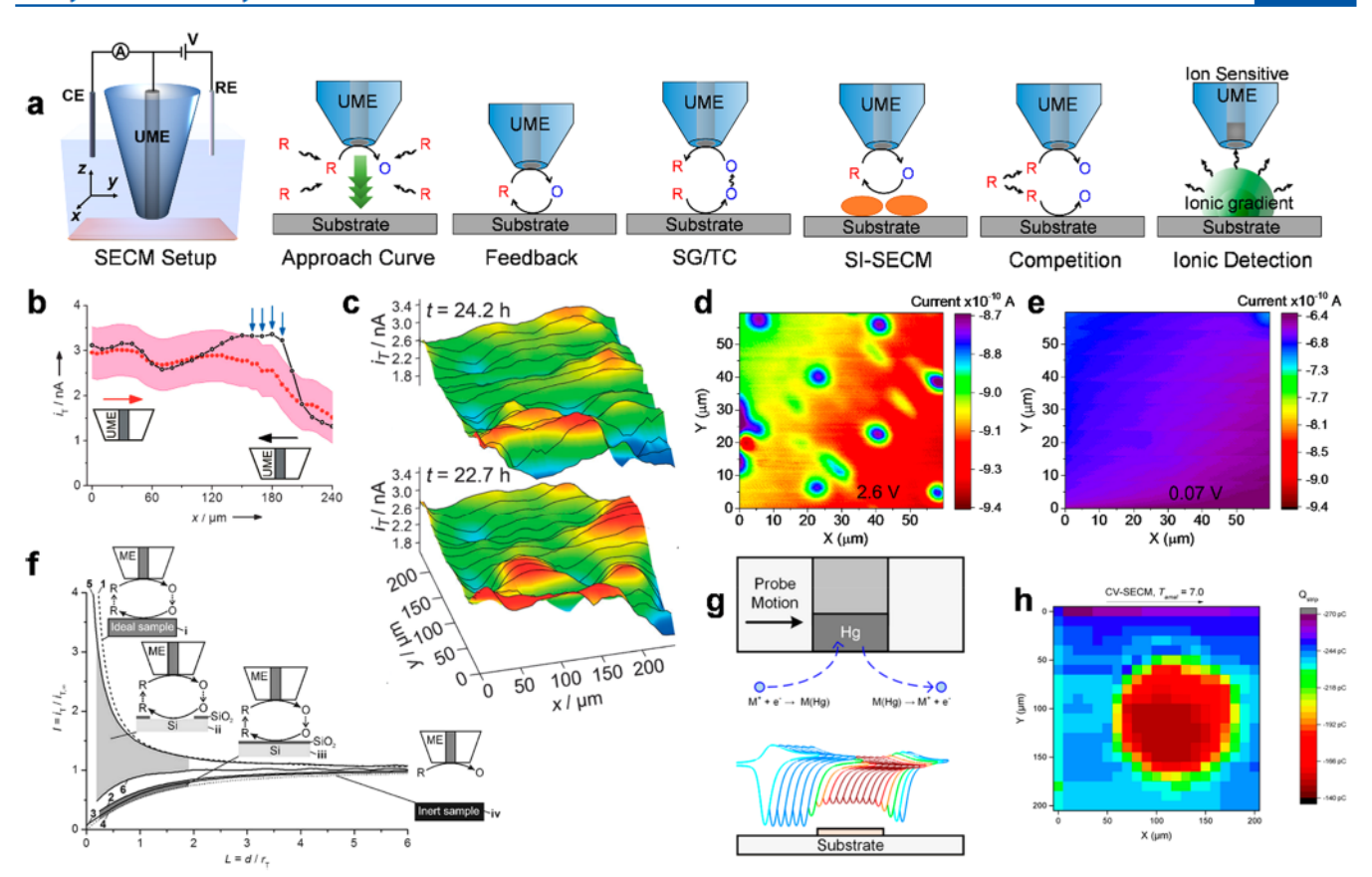


Figure 2. SECM modes to study the electrochemical interface. (a) Schematics of SECM setup and its different operation modes. Data shown in (b) and (c) represent stability studies of a formed SEI layer on graphite. (b) Determination of short-term SEI stability by comparing consequent forward and backward line scans. The mismatched location in the trace—retrace indicates the local SEI fluctuation within several minutes. (c) Determination of long-term SEI variation by a series of SECM feedback images taken at different times. (d, e) SECM feedback images at various FLG potentials listed in each panel; the current changes reflect the changes in substrate kinetics following SEI formation. (f) Determination of Si anode surface kinetics via SECM approach curves: 1, pure positive feedback; 2–3, Si surface with intact native oxide layer; 4, pure negative feedback; 5–6, Si surface with damaged native oxide layer. (g) Schematics of Hg disk-well ionic probe and its working principle. (h) CV—SECM data collected at Hg disk-well UME; the integrated stripping charge is extracted and plotted here. UME, ultramicroelectrode; RE, reference electrode; CE, counter electrode; ME, microelectrode. Parts (b) and (c) reproduced from Spatiotemporal Changes of the Solid Electrolyte Interphase in Lithium-Ion Batteries Detected by Scanning Electrochemical Microscopy, Bülter, H.; Peters, F.; Schwenzel, J.; Wittstock, G. Angew. Chem., Int. Ed. 2014, S3, 10531–10535 (ref 90). Copyright 2014 Wiley. Parts (d) and (e) reproduced from Hui, J.; Burgess, M.; Zhang, J.; Rodriguez-López, J. ACS Nano 2016, 10, 4248–4257 (ref 35). Copyright 2016 American Chemical Society. Part (f) reprinted with permission from J. Electrochem. Soc. 2016, 163, A504–A512 (ref 91). Copyright 2016, The Electrochemical Society. Parts (g) and (h) reproduced from Barton, Z. J.; Rodriguez-López, J. Anal. Chem. 2017, 89, 2716–2723 (ref 92). Copyright 2017 American Chemical Society.

ADVANCED ELECTROCHEMICAL SCANNING PROBE MICROSCOPY

Scanning electrochemical probe microscopy (SEPM) is another large family of analytical tools for energy storage material interfaces, including scanning electrochemical microscopy (SECM), scanning ion conductance microscopy (SICM), scanning micropipette contact method (SMCM), and scanning electrochemical cell microscopy (SECCM). Other in situ scanning probe microscopy (SPM) tools, such as atomic force microscopy (AFM), electrochemical strain microscopy (ESM), and scan tunneling microscopy (STM), have also been applied in energy storage studies. Compared to the bulk electrochemical analysis techniques discussed in the previous section, scanning probe techniques provide specific electrochemical information with high temporal and spatial resolution over the substrate of interest. These techniques quantify the highly localized information about substrate heterogeneity, electron transfer kinetics, redox species generation and uptake, morphological changes, and ionic fluxes (Figure 2), which help us better understand surface properties and interfacial reactions of energy storage materials.

Scanning Electrochemical Microscopy. Ever since its introduction in 1989, ⁸¹ SECM has gained tremendous attention as a powerful electrochemical scanning probe technique to study interfacial processes for energy storage systems, ^{82,83} electrocatalysis, ^{84,85} charge transfer kinetics, ^{86,87} and biological systems. ^{88,89} In SECM studies, an ultramicroelectrode (UME) is positioned close to a substrate surface immersed in solution to characterize the electrochemical processes and structural differences (Figure 2a). The measured current at UME usually depends on the rate of active component fluxes (electrons or ions), tip—substrate distances, and substrate reactivity. While the tip can be approached to the substrate in the *z*-direction to obtain local electron transfer kinetics, it can be also scanned along *x*- and *y*-directions at constant *z*-location to obtain areal mapping of specific electrochemical information at the substrate surface and the topographical changes.

SECM Operation Modes. SECM can be operated in multiple modes to collect information of interest at energy storage interfaces, as described in Figure 2a. These modes highly depend on the tip—substrate potential and their distances. To simplify the schematic representation of SECM, we assume that only the reduced species "R" initially exist in solution, and "R" can provide an electron to generate oxidized species "O". Note that there is already a comprehensive review discussing the working principles and experimental design of SECM by Polcari et al. Herein, we only focus on detailed applications for interfacial processes of energy storage systems and the specific information that can be gained from these SECM modes. Important operational modes and concepts of SECM are summarized below.

- (i) Approach Curve. The approach curve is performed by holding a constant potential (or open circuit) at the UME while approaching the substrate surface and tracking the current—distance relationship. Often, highly reversible species with fast kinetics (e.g., Ferrocene) are used as a source of current. By fitting the approach curve, information such as tip—substrate distance and localized heterogeneous electron transfer rates of substrate underneath the UME can be obtained. Hence, useful information such as changes in sample thickness to surface kinetics can be monitored with this method. Alternatively, approach curves can be used for making soft contact with microand nanosized particles for single particle electrochemical measurements.
- (ii) Feedback Mode. Once approached to the surface, the UME is raster-scanned over the sample surface at a constant z-position. Generally, a bias is applied to the probe to activate an electrochemical reaction of a selected redox mediator. The collected faradaic current at the tip directly correlates with the topography of a substrate and its ability to activate reversed reactions of the tip-generated redox mediators. Hence, this method is commonly used to study the short- and long-term stability of the SEI ^{98,99} and the effects of electrode material, ¹⁰⁰ solvent, electrolyte, ¹⁰¹ and additives, as well as substrate topography. ¹⁰²
- (iii) Substrate-Generation/Tip-Collection Mode. In substrate-generation/tip-collection (SG/TC) mode, the redox active species are generated at the substrate and collected at the tip amperometrically or potentiometrically. In this mode, tip current depends on the chemical profile and concentration of species generated at the substrate. This method can be used to identify the intermediate formation at different substrate conditions, as well as quantify its generation rate. 103
- (iv) Competition Mode. In competition mode, both tip and substrate are activated to consume the same electrochemically active species. The tip current depends on the tip—substrate distance, collection efficiency, and rate of competition reactions at the substrate. This method can be used to observe the active species consumption at the substrate. 104
- (v) Surface Interrogation-SECM Mode. In surface interrogation-SECM (SI-SECM) mode, the tip is biased to generate the electroactive mediator which is used to titrate bound interfacial species at an unbiased or insulating substrate. This method can be used to quantify the charge and reaction kinetics of those species¹⁰⁵ and even thin-film charge storage entities.⁹⁷
- (vi) Ionic Detection. This is a newly developed operation mode utilizing Hg-based ionic sensitive probes to quantify local ionic flux changes. The localized ion uptake and release can be monitored with this method without the need of a redox active mediator. ¹⁰⁶

Redox Reactivity. SECM has a broad applicability to explore the formation and properties of the SEI for alkali-ion battery systems. As mentioned previously, the SEI is an electronically passivating layer formed on an anode surface during the initial cycling of the battery. 30 The distinct activity differences between the conductive electrode surface and the insulating SEI deposits makes the SECM a compelling tool to study the SEI formation and stability. Bülter et al. demonstrated the use of feedback mode SECM to investigate the spatiotemporal properties of SEI formed on graphite composite electrodes.⁹⁰ In their study, they used forward and backward line scans (Figure 2b) to evaluate short-term fluctuations in the SEI and SECM feedback images at different times to evaluate long-term changes (Figure 2c). They observed SEI instability and considered graphite particle volume expansion, binder swelling, and mechanical stress relaxation as potential suspects. Conversely, the SEI formed on a charged graphite anode after rinsing exhibited a nonuniform and destabilized behavior in an SECM feedback study.⁹⁸ This emphasized the need of a properly designed transfer procedure for ex situ studies of SEI properties. Using similar strategies, Bülter et al. studied the local variation of SEI formed on Li-metal anode. 102 Compared to previous work on lithiated graphite, 90 a similar range of electron transfer rates of the SEI layer was found on Li with a lower frequency of short-term fluctuations. The effect of carbon materials on SEI properties was also studied by Bülter et al. as well.⁹⁹ Highly oriented pyrolytic graphite (HOPG) demonstrated a more stable SEI passivation over a time scale of hours compared to graphite composite electrode. They suggested the effect of particle-particle interaction and electrolyte-binder interaction might have a negative effect on the SEI stability. Using the SECM approach curve mode, Bülter et al. obtained the local kinetics and thickness changes of soaked graphite electrode. 95 An 11% swelling ratio was observed for the graphite composite, and the majority of the swelling was proved to be polyvinylidene fluoride binder contribution.

Other than the stationary evolution of SEI studied above, it is important to monitor the kinetic changes and intermediates generation during the SEI formation process. Zampardi et al. tracked the normalized feedback current changes at the UME while performing CV on glassy carbon electrodes where the SEI was formed in an ethylene carbonate (EC) and diethyl carbonate (DEC) mixture. 107 They determined the formation onset potential of SEI at 0.8 V vs Li+/Li and found the use of different cations (Li+, TBA+, and Na+) had no impact on the insulating properties of the SEI. In contrast, the addition of 2-5% vinylene carbonate (VC) shifted the onset of SEI formation on the graphite composite electrode to 0.5 V positive. 101 However, the formation of the early VC-based SEI layer did not suppress further electrolyte decomposition at more negative potentials, and a final product of SEI insulating layer formed on the graphite anode.

Typically, graphite composite electrodes undergo large topography changes at the tens of micrometers scale. This large variation in topography makes higher resolution, nanoscale SECM difficult with traditional methods. Patterned, planar FLG can be used as a model platform to simulate SEI formation processes on graphite with improved contrast and resolution. As shown in Figure 2d,e, a gradual passivation of the FLG occurred as it was biased more negative during SECM feedback imaging. A complete SEI layer eventually covered the FLG surface to totally block the electron transfer as observed by SECM.

Other than determining the surface activity changes during SEI formation, SECM SG/TC mode can be used to analyze SEI species formation at different potential regions. Qian et al. demonstrated the use of propylene carbonate for artificial SEI formation for Li-metal anode. The radical anion and alkylcarbonate formation was observed at high and low potential stages, respectively. 103 During the LIB cycling, a cathode electrolyte interphase (CEI) layer was found at the cathode surface. 108 The proper CEI passivation is critical for improving the long-term cyclability of high voltage cathodes. 108 The properties of the CEI have been studied via SECM feedback mode as well. 100 Unlike the insulating SEI layer formed on anodes, conductive CEI can be found on cathodes. With SECM imaging before/after cycling, Zampardi et al. confirmed that a conductive CEI had formed at the lithium metal oxide cathode as indicated by the positive feedback behaviors. 100 While similar components were discovered for both SEI and CEI, e.g., LiF, alkylcarbonate, and Li_2CO_3 , future studies are required to unravel the origin of different electronic properties between

The SEI properties of other LIB anodes, e.g., Si and TiO_2 , have been explored with SECM as well. The existence of a native SiO_2 layer passivation on a Si surface has been verified. Mechanical or chemical removal of the native oxide to expose underlying Si results in strongly enhanced kinetics (Figure 2f). The SEI formed on the Si anode is also an electronic insulating layer. The SEI formed on the Si anode is also an electronic insulating layer. However, the large volume expansion of Si during lithiation causes crack formation and results in discontinuity to the SEI and increased reactivity at the defect areas. Recently, SEI development was evaluated on an anatase TiO_2 anode at various potentials using SECM feedback. The positive feedback results revealed the apparent SEI had no effect on the electron transfer properties of the TiO_2 , in contrast with traditional carbon-type LIB anodes. TiO_2

SECM approach curves have been used to determine heterogeneous charge transfer kinetics for other energy storage interfaces. This method can potentially be applied to analyze and screen suitable redox mediator additives for redox-active electrolyte supercapacitors with improved energy densities, 111 as well as proper homogeneous oxidizing agents to recycle Li₂O₂ and sustain its high cycling rate in Li–O₂ batteries. 96 Pulsed amperometric detection methods can be used to study soluble reactive oxygen species above gas-diffusion electrode. 98 The tip–substrate distance correlation of O₂ and O₂ $^{\bullet-}$ concentration was previously investigated as well. 112

Mapping Ionic Processes. Proper design of redox mediator or probe material grants access to ionic measurements at the UME. Matching the Nernst potential of redox mediator and Fermi level of active electrode material has been used to monitor the (de)intercalation kinetics at LIB cathode. 113 Using SECM feedback mode with FcBr₂⁺ and Fc as Li⁺-coupled redox shuttle mediators, Yan et al. 113 demonstrated reaction coordinate dependent, interfacial charge transfer kinetics upon (de)lithiation on LiFePO₄/FePO₄. While this method provides only indirect information on Li+ changes, replacing the traditional UME with a Hg-based ionic sensitive probe provides more direct determination of alkali-ion fluxes at a functioning electrode (Figure 2g).¹¹⁴ This Hg-based probe utilizes the amalgamation and stripping processes of Hg to quantify ion specific information of alkali-ions, including flux changes, and they are compatible for high concentrations and long time scales operation without sacrificing the image resolution. 92,115 A CV-SECM method is typically applied when using Hg-based UMEs,

where the individual CVs are obtained at each pixel of the SECM image. Changes in amalgamation (stripping) current and stripping charge can be used to extrapolate the localized ionic flux upon substrate reactions or topography differences (Figure 2h). Through the use of a Hg-based UME and the CV-SECM method, Hui et al. recognized the preferred ionic channel for Li+ intercalation at a patterned FLG edge plane under constant bias of 0.07 V vs Li⁺/Li.³⁵ After further positioning the Hg-based UME at locations above both basal and edge planes, they distinguished the two regions through an observed decrease in both amalgamation and stripping peaks at only the edge planes when applying progressively negative potentials where intercalation occurs. This study verified the Li⁺ intercalation process occurs only at the edge plane of graphitic materials. Barton et al. applied the Hg disk-well probe to measure the reversible K+ (de)intercalation at HOPG edge planes. They were able to track the substrate's electronic response after initial SEI formation and the ionic response during substrate intercalation with this technique. 106 Aside from intercalation materials, redox active polymers are novel materials for energy storage in redox active flow batteries (RAFB). Elucidating the interaction between electrolyte and redox active polymers in these systems is a complex but important issue. Using SI-SECM, Burgess et al. observed a 40 times enhancement in redox kinetics induced by strong poly(para-nitrostyrene) and K⁺ interactions compared to TBA+ and Li+ cations. This K+ uptake by the polymer film was later confirmed by Hg probe SECM as well. 10

In addition to the traditional methods, SECM can be coupled with other techniques for multifunctional testing. 82,116 Clausmeyer et al. coupled SECM with surface-enhanced Raman scattering to characterize local modifications of the electrified interface by a self-assembled monolayer. 117 Simultaneous SECM-Raman analysis has been employed to determine FLG heterogeneities and interfacial reactions with high temporal rate and sub-10 µm resolution. 116 Upon FLG oxidation, the exfoliation and passivation layer formation were tracked via Raman signatures, along with surface activity changes monitored with SECM. This method is a powerful candidate for energy storage purposes with spatiotemporally correlated electrochemical and spectroscopic information. 116 Gossage et al. applied contact mode SECM and Raman coupled surface interrogation SECM (SI-SECM) to elucidate the capacity, redox active motif concentration, interparticle diffusion coefficient, and reaction mechanism of a single flowable energy storage entity-redox active colloid for RAFB.⁹⁷

Limitations and Future Directions. Improvements in SECM methodology and capabilities are needed for analyzing complex battery interfaces. As we mentioned above, SECM tip current depends on both tip-substrate distance and substrate activity. For typical SECM images operated at constant z-location, the collected feedback currents are convoluted results from both substrate heterogeneous activity and topography. The lack of monotonous signal for tip-substrate distance responses makes potentiometric SECM imaging difficult to operate at a constant tip—substrate distance. However, a couple of approaches can be used to solve this problem including coupling with other SEPM techniques to delineate distance from electronic/ionic properties and obtain simultaneous electronic and ionic information at a controlled tip-substrate distance. More detailed information can be found in the SICM section below. Tilting the substrate to make the entire surface perpendicular to the UME is another limitation with SECM because it can be tedious and timeconsuming. Recently, Barforoush et al. demonstrated a new

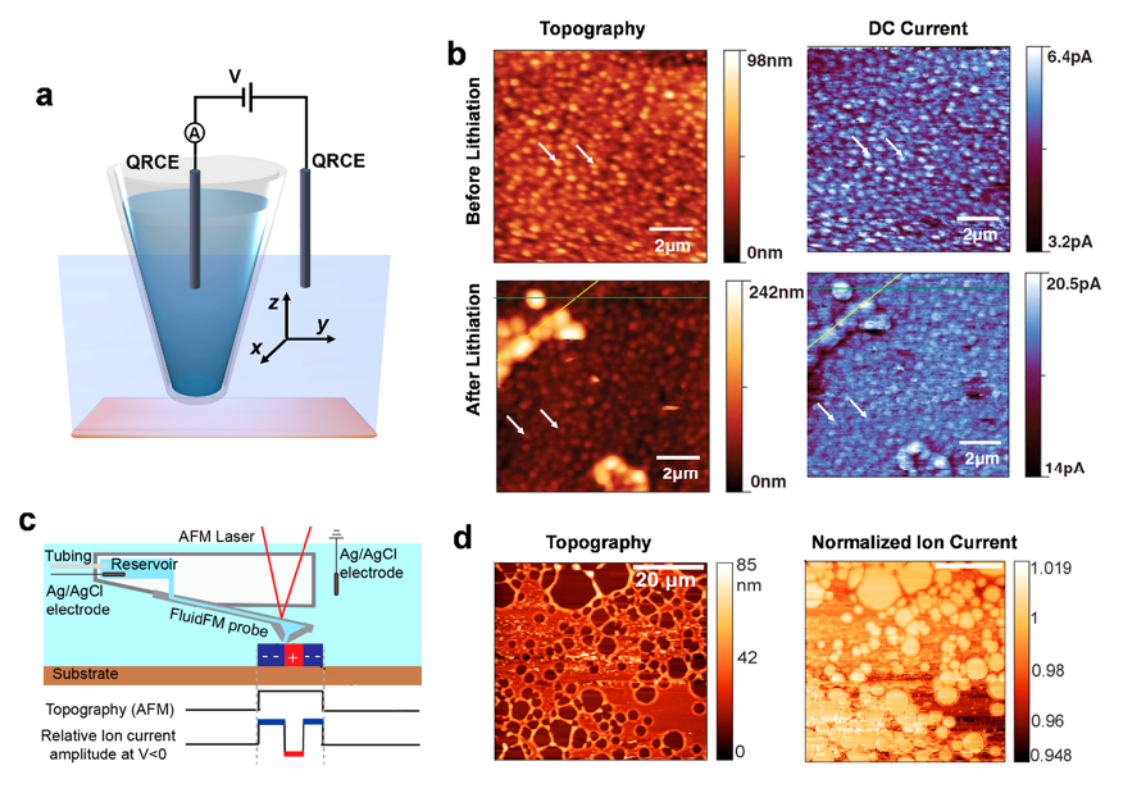


Figure 3. SICM modes to study the electrochemical interface. (a) Schematics of SICM setup. (b) SICM topography and DC current images of a 60 nm-thick Sn thin film before and after lithiation. (c) Schematic representation of the AFM—SICM setup and operation principle over a charged feature on the substrate. (d) AFM—SICM simultaneous topographical and ion current imaging of a partial polystyrene film on glass. The current is normalized to the current on the glass at contact. Part (b) reproduced from Nanoscale *In Situ* Characterization of Li-ion Battery Electrochemistry Via Scanning Ion Conductance Microscopy, Lipson, A. L.; Ginder, R. S.; Hersam, M. C. *Adv. Mater.* 2011, 23, 5613—5617 (ref 128). Copyright 2011 Wiley. Parts (c) and (d) reproduced from Dorwling-Carter, L.; Aramesh, M.; Han, H.; Zambelli, T.; Momotenko, D. *Anal. Chem.* 2018, 90, 11453—11460 (ref 129). Copyright 2018 American Chemical Society.

fuzzy logic algorithm to automatically and accurately align tip—substrate to generate constant height images. 118

Another limitation of SECM is the relatively slow imaging speed, which restricts the temporal resolution of SECM. Since the SECM monitors the diffusion controlled feedback current, a relatively slow imaging rate is usually applied to avoid disturbance of the solution. 119 Kuss et al. provided the numeric modeling and experimental proof of kinetics information extrapolated for high speed (50 µm/s) scanning at constant height with forced convection. 120 Integrating several probes together is a practical method to obtain multifunctional electrochemical characterization with high speed. In this case, the tip geometry determines the readout at each probe. Stephens et al. provided 3D finite element modeling of dual-barrel UME with various geometries and tip-substrate distances and suggested suitable experimental conditions for each case as well. 121 Recently, 3D printing technology has been applied to fabricate low-cost SECM instruments with adequate spatial resolution.122 With these development in theory and instrumentation, we foresee the SECM will further expand its applicability in energy storage systems and beyond.

Scanning Ion Conductance Microscopy. Another important technique of the SEPM family is SICM, which was first discovered by Hansma et al. in 1989. In contrast to SECM, SICM utilizes a micro- or nanopipette as a probe for the detection of ionic current. A typical setup for SICM is shown in Figure 3a, where both substrate and the nanopipette are immersed in electrolyte solution. Two quasi-reference counter electrodes (QRCE, e.g., Ag/AgCl) are used. One of them is

placed inside of the nanopipette probe, which back filled with electrolyte, and the other one is placed in the bulk solution. The ionic current flow between the two biased QRCEs is measured. This ionic current is determined by the pipet pore and tip—substrate distance. More detailed instrumentation and operation theory can be found in previous reviews. The nanopipette is usually fabricated with a laser puller to dimensions of tens of nanometers, yielding nanometer-sized SICM resolution. Hence, SICM is a powerful technique for high resolution, noncontact detection of substrate topography and local ionic flux. SICM has broad applications for noninvasive imaging of living cells 126 and surface-interface charge determination. 127

Topography and Ionic Conductance Detection. Ionic processes are often important to operating energy storage material interfaces, e.g., Li+ uptake at LIB electrodes and ion migration and adsorption at supercapacitor surfaces, making SICM an important technique for these applications. The first application of SICM to the LIB field was done by Hersam and co-workers. 128 Two types of signals were collected in this experiment, alternating current (AC) and direct current (DC). The SICM tip was oscillated vertically to approach the substrate, and the magnitude of the AC current depended on the tipsubstrate distance. Hence, the AC component provided topography feedback, and the DC component could be used for measuring localized electrochemical changes. With both AC and DC signals, the authors studied a 60 nm deposited tin thin film upon lithiation. Compared to the uncharged state, the lithiated tin particles displayed increased height at certain active

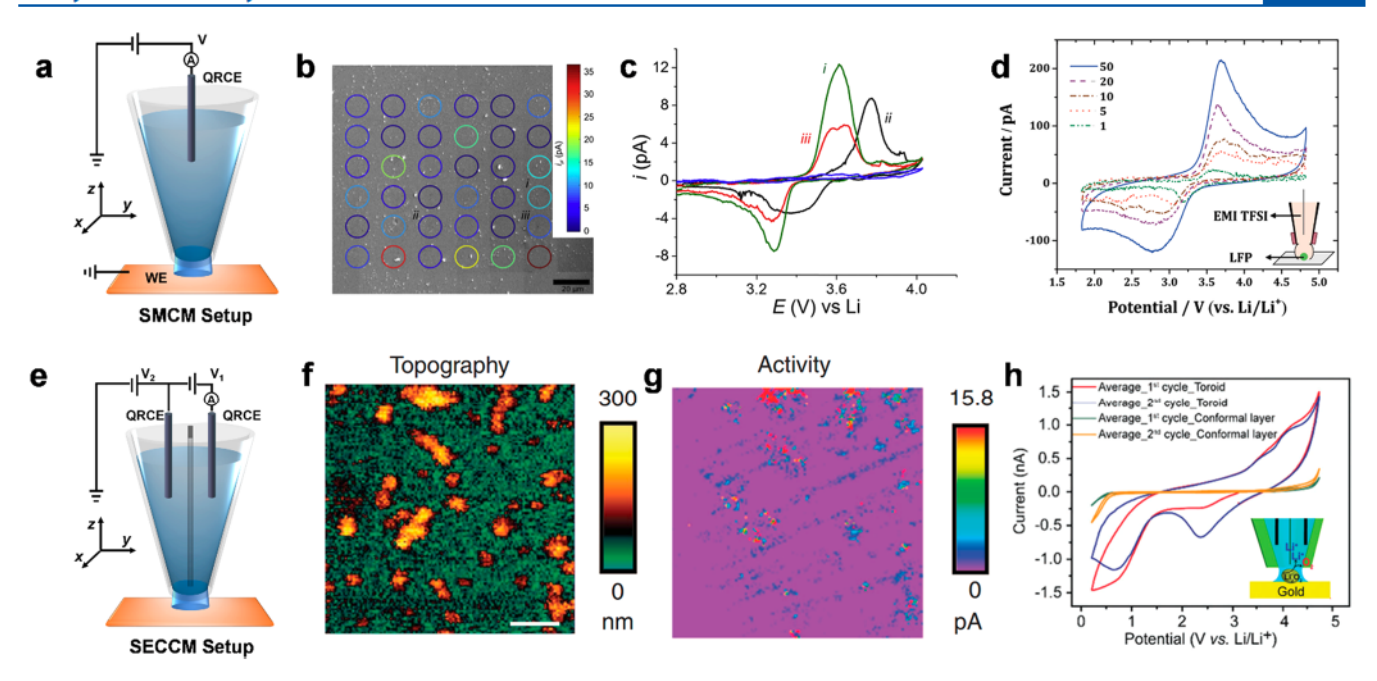


Figure 4. Droplet-based SEPM modes to study the electrochemical interface. (a) Schematics of SMCM setup. (b) Deintercalation peak current distributions of LiFePO₄ particles dispersed at Au substrate obtained via SMCM. The circles represent the wetted area of SMCM pipet, with the colors indicating the peak current at each location. (c) CV responses of various grid location indicated in panel b, with the blue curve representing the background tested at Au substrate. (d) Scan rate-dependent CVs of LiFePO₄ particles dispersed at glassy carbon substrate. (e) Schematics of SECCM setup. (f, g) Simultaneous SECCM topography (f) and activity (g) images of LiFePO₄ nanoparticles on Pt substrate. (h) Average CVs of toroid and comformal layer structured Li₂O₂ grown on Au substrate. EMI TFSI, 1-ethyl-3-methylimidazolium bis(trifluoromethylsulfonyl)imide; LFP, lithium iron phosphate. Parts (b) and (c) reprinted from Measurement on isolated lithium iron phosphate particles reveals heterogeneity in material properties distribution, Snowden, M. E.; Dayeh, M.; Payne, N. A.; Gervais, S.; Mauzeroll, J.; Schougaard, S. B. J. Power Sources 2016, 325, 682–689 (ref 138). Copyright 2016, with permission from Elsevier. Part (d) reproduced from Dayeh, M.; Ghavidel, M. R. Z.; Mauzeroll, J.; Schougaard, S. B. ChemElectroChem 2018, 5, 1–8 (ref 139). Copyright 2018 Wiley. Parts (f) and (g) reprinted by permission from Macmillan Publishers Ltd.: Nature Communications, Takahashi, Y.; Kumatani, A.; Munakata, H.; Inomata, H.; Ito, K.; Ino, K.; Shiku, H.; Unwin, P. R.; Korchev, Y. E.; Kanamura, K.; Matsue, T. Nat. Commun. 2014, 5, 5450 (ref 140). Copyright 2014. Part (h) reproduced from E, S. P.; Kang, M.; Wilson, P.; Meng, L.; Perry, D.; Basile, A.; Unwin, P. R. Chem. Commun. 2018, 54, 3053–3056 (ref 141), with permission of The Royal Society of Chemistry.

regions (Figure 3b). The AC–DC correlation also suggested a rapid growing film formation at the tin surface during lithiation. Later, Lipson et al. applied SICM to LIB MnO electrodes and studied the SEI inhibition properties of atomic layer deposited Al₂O₃ thin film by tracking the topography change before/after lithiation. ¹³⁰

Understanding the properties of Li⁺ adsorption and transport at nanostructured interfaces is beneficial for the modeling of energy storage systems. Using SICM, Plett et al. studied the ionic current rectification of polycarbonate nanopores in commonly used LIB solutions with LiClO₄ in propylene carbonate. 131 They attributed this rectification to the adsorption of Li⁺ at the pore surface, as well as the ion adsorption induced finite dipole moment at nanopore walls. Utilizing the surfaceinduced rectification phenomenon, Dorwling-Carter et al. introduced an AFM-SICM coupled design for simultaneous imaging of sample topography and surface charge (Figure 3c). 129 Taking advantages of the AFM feedback loop, the authors were able to independently collect the surface charge of a polystyrene/glass substrate at high speed (Figure 3d). In principle, these studies open up possibilities of electrical double layer characterization at supercapacitor interfaces.

Limitations and Future Direction. Despite the high resolution topography imaging capability of SICM provided in previous publications, none of them discussed an accurate investigation of the chemical species and kinetics involved in the surface processes. Although Kang et al. demonstrated the application of SICM to visualize the topography and electro-

chemical activity of electrocatalytic nanoparticles, ¹³² this is still an indirect and nonspecific measurement of sample kinetics. One of the common solutions to the problem is the coupled SICM-SECM technique. Combining the advantages of SECM and SICM, the simultaneous detection of sample topography, ion conductance, and charge transfer kinetics can be achieved. There are several reported methods to fabricate different geometries of SICM-SECM tips, including a metal nanoring coating on the nanopipette, ¹³³ a crescent-shaped metal coating on the nanopipette, ¹³⁴ and dual- or quad-barrel geometries. 135,136 We foresee the coupling of SICM-SECM techniques will have more applications for interfacial electronic and ionic processes at battery electrode-electrolyte interfaces. Note that probes deviating from traditional disk-type geometries might lead to complications and artifacts for the SECM readout; 121 precautions and proper data analysis methods are needed for future application of energy storage interfaces.

Scanning Micropipette Contact Method. SMCM was developed by Unwin and co-workers in 2009. ¹³⁷ As shown in Figure 4a, a micropipette filled with an electroactive mediator and electrolyte solution is used as the probe in this system. When the micropipette is brought close to the substrate surface, a micrometer-thick liquid meniscus forms between tip and substrate surface. The current is measured between the substrate working electrode and the reference-counter electrode inside the micropipette. ¹³⁷ Compared to SECM and SICM where the entire substrate is immersed in solution, SMCM characterizes the confined electrochemical reactions limited by the contact

area between droplet and substrate. The easy fabrication of micropipettes via laser pulling and the ability to make individual measurement of specific sample location make SMCM a powerful tool for quantification of electrode activities. Using SMCM, Snowden et al. was able to analyze the isolated LiFePO₄ particles on a Au surface without binder and carbon additives' interference at c.a. 10 μ m resolution (Figure 4b,c). Their work investigated the variation in LiFePO₄ particle sizes and the heterogeneous activities via combined SEM and SMCM analysis. Dayeh et al. introduced the use of 1-ethyl-3-methylimidazolium ionic liquid to further expand the SMCM operation potential window for high redox potential cathode materials. The lithiation/delithiation property of LiFePO₄ and LiNMC were characterized in this study with close to single cluster detection (Figure 4d).

Scanning Electrochemical Cell Microscopy. In the SMCM technique, it is difficult to maintain constant height imaging with the same contact area meniscus. SECCM is an advanced version of SMCM with the capability for high resolution topography and electrochemical imaging. 142 The instrumentation and theory have been described in a previous review. 143 In general, the SECCM setup consists of a dual-barrel pipet and two QRCEs in each barrel; a voltage difference is applied between two QRCEs, and the tip is modulated sinusoidally normal to the substrate. Both DC component (ionic current) and AC component (formed due to droplet meniscus oscillation frequency) are collected during the experiment (Figure 4e). Similar to SICM approaches, the detection of AC current in SECCM leads to a precise control of tip-substrate separation. The activation of substrate is not required in SECCM; hence, it further expands the application of SMCM to insulator materials.

The SECCM technique has been previously used to image the electrochemical activity of graphene and graphite materials at 100 nm spatial resolution. ¹⁴⁴ This study identified the step edge of HOPG as well as characterized the thickness-dependent charge transfer kinetics of an exfoliated graphene sample. This offers the opportunity to use SECCM for characterization of carbon material surfaces used in energy related studies. Using high resolution single channel SECCM, Takahashi et al. visualized the topography and heterogeneous (de)intercalation activity change of LiFePO₄ cathode down to single particle level (Figure 4f,g). 140 Likewise, the charge-discharge activity of toroidal and conformal layer Li2O2 formed on Au electrode using voltammetric SECCM for Li-O₂ battery applications was described recently.141 The toroidal Li2O2 displayed higher electrodissolution rate and activity toward a layered structure (Figure 4h). This work also highlighted the use of a polymer gel in organic solutions to control the wetting and contact of the meniscus at the tip end, which makes future application of a nonaqueous energy storage system plausible. SECCM has also been applied in dye sensitized solar cells (DSSCs). 145,146 Aaronson et al. 145,146 studied the charge transfer kinetics of an I₃⁻/I⁻ DSSC redox shuttle at a polycrystalline Pt surface and correlated an observed kinetics difference with the grain orientation. Photoactivity mapping of TiO2 aggregates (DSSC photoanode) was demonstrated via SECCM as well. These studies describe the wide applicability of SECCM for comprehensive understanding of interfacial processes and environments of batteries and DSSCs.

Advantages and Limitations. Compared to SECM and SICM, where the detecting probes are immersed inside the solution with the substrate, droplet-based SEPMs have a

confined meniscus contact area forming a localized electrochemical cell. With this design, the unwanted detection from surrounding areas can be eliminated, thus increasing the signalto-noise. Furthermore, Momotenko et al. introduced a high speed SECCM imaging mode of 8000 image pixels per second. 147 This was achieved using a preacquisition of topography at an initial slow scan, followed by a series of quick spiral-type retraces with recorded spatial coordinates. All of these properties make SECCM an arising technology for future perspectives of the energy storage interface. We should mention that currently most of the SECCM studies are done by filling a pipet with aqueous solutions. However, the majority of energy storage systems, e.g., LIBs, operate in organic solutions for their expanded potential windows. The overwetting of organic solution to the substrate might be difficult to manage. A few proposed solutions are to use either ionic liquids as a solvent 139 or polymer gel to enhance solvent viscosity. 141 Still, none of these are perfect solutions for in situ SECCM study in real battery conditions. Moreover, the limited solvent loading inside the pipet and evaporation at micrometer-sized liquid droplets makes SECCM difficult for long-term characterization of interfacial processes.

Other Electrochemical Coupled Scanning Probe Microscopy. Coupled with electrochemical setup, conventional SPM techniques, e.g., AFM and STM, have been widely applied for in situ characterization of the morphological, electrical, and mechanical properties of LIB anode and cathode materials. Here, we only highlighted several recent developments of multifaceted SPM studies for LIB systems, as well as emerging energy storage materials and systems beyond LIB.

In Situ AFM for LIB Anode. AFM is generally accepted as a powerful tool for diversified tip-substrate interactions detection, which has been applied to visualize and analyze the SEI formation mechanism, ¹⁵³ influences of additives on SEI passivation, ^{154,155} new SEI design principles, ¹⁵⁶ and solvent cointercalation processes³¹ at LIB anodes. Recently, multiple in situ AFM studies were focused on the influence of fluoroethylene carbonate (FEC) electrolyte additives on the SEI, which were proved to enhance the stability and cyclability of the LIB anode. IST Shen et al. found the top layer SEI on HOPG formed in EC consisted mainly of alkyl carbonate-based scattered islands, while in FEC this layer is LiF-based and more thick and densely packed. 158 Similar compact structures were found on an Fe₃O₄ anode. The FEC electrolyte can inhibit the surface decomposition on Si anode as well. 160 Haruta et al. observed a uniform morphology and limited electrolyte deposition at a LiF artificial SEI coated Si surface. 160 This LiFrich SEI formed in FEC electrolyte was further proven to prevent Li dendrites formation at a graphite surface. 161 NaF-rich SEI formed in Na+ containing electrolyte with FEC additives was found to stabilize the Na dendrites formations on the Au current collector as well, suggesting a suitable surface treatment for Na metal anode.162

Understanding the SEI properties on Si anodes provided guidance for a new category of alloy-based LIB anode designs. Tokranov et al. analyzed the SEI formation on patterned Si anodes with a single lumped parameter-based model. They reported a scan rate-dependent initial SEI feature formed during the first cycle, where fast scan rate leads to a thin and smooth SEI formation. This new SEI typically forms at cracking and delamination location of the initial SEI layer due to lithiation induced Si expansion. With an Al₂O₃ passivation layer coating

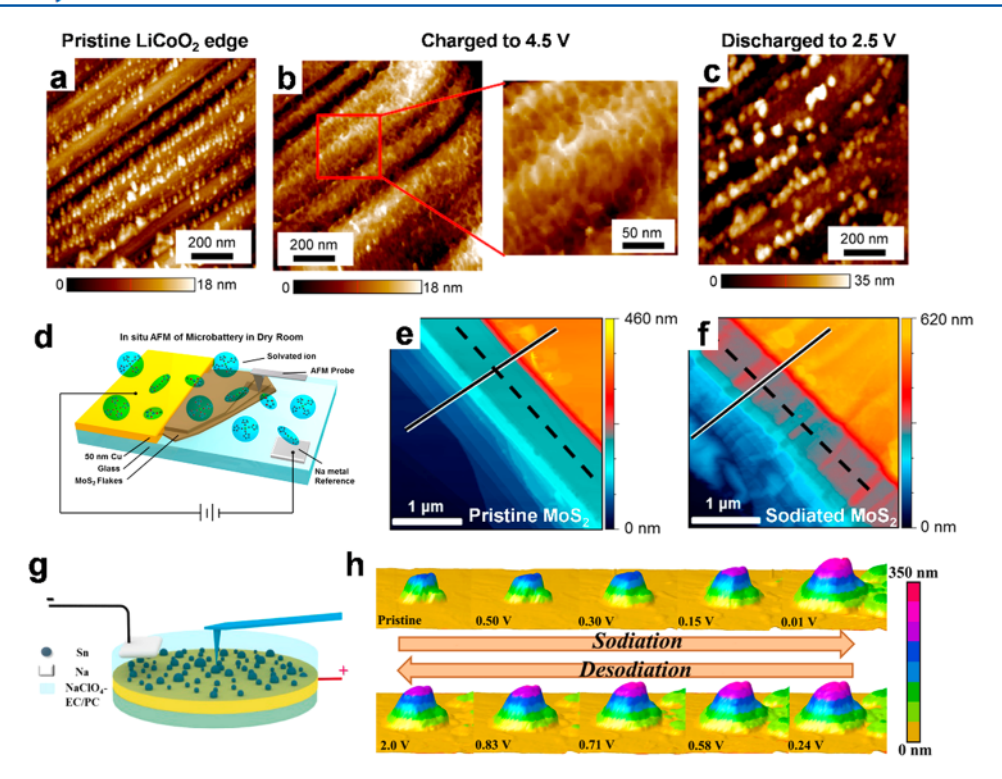


Figure 5. Electrochemical coupled AFM to study the electrochemical interface. (a-c) AFM images of CEI formation at LiCoO₂ edge planes, at pristine (a), charged to 4.5 V (b), and fully discharged (c) conditions. (d) Schematics of the planar MoS₂ microbattery analyzed by in situ AFM. (e, f) AFM images of MoS₂ flake before (e) and after (f) sodiation. (g) Schematic of single Sn nanoparticles anode analyzed by in situ AFM. (h) 3D AFM topography changes of one Sn nanoparticle upon sodiation and desodiation. Parts (a-c) reproduced from Lu, W.; Zhang, J.; Xu, J.; Wu, X.; Chen, L. ACS Appl. Mater. Interfaces 2017, 9, 19313–19318 (ref 150). Copyright 2017 American Chemical Society. Parts (d-f) reproduced from Lacey, S. D.; Wan, J.; Cresce, A. v. W.; Russell, S. M.; Dai, J.; Bao, W.; Xu, K.; Hu, L. Nano Lett. 2015, 15, 1018–1024 (ref 151). Copyright 2015 American Chemical Society. Parts (g) and (h) reproduced from Han, M.; Zhu, C.; Zhao, Q.; Chen, C.; Tao, Z.; Xie, W.; Cheng, F.; Chen, J. ACS Appl. Mater. Interfaces 2017, 9, 28620–28626 (ref 152). Copyright 2017 American Chemical Society.

on the Si pattern, the authors were able to observe the clearly discernible lithiation front moves in from the edge plane. Huang et al. determined the morphology and Young's modulus for the SEI at Si anodes. They found a thick and soft SEI layer formation at micrometer-sized Si particles, which undergoes multiple expansion and contraction processes. In contrast to that, no volume change was observed at nanosized Si particles upon (de)lithiation; hence, its SEI is comparably thinner and harder than its micrometer-sized counterpart.

In Situ AFM for LIB Cathodes. The multifunctional SPM techniques are also engaged in LIB cathode characterization. Using ex situ amplitude modulation and frequency modulation (AM-FM) and kelvin probe force microscopy (KPFM), Wu et al. were able to visualize the changes of LiCoO2 cathode upon cycling, including irreversible size expansion, stiffness loss, and surface potential reduction. 165 The surface morphology changes of Li-metal oxides during reversible CEI formation and decomposition can also be monitored via in situ AFM. 150 For LiCoO₂ a loose fibrillar structure CEI formed only at the edge plane of the LiCoO₂ crystal but not the basal plane (Figure 5a c). The authors pointed out that the exposed cobalt-ion at the edge plane might serve as a plausible CEI formation catalyst. Yang et al. determined the temperature-dependent Li⁺ diffusion coefficient and corresponding activation energy of a Li-rich LiNMC cathode via electrochemical strain microscopy (ESM), 166 which in magnitude is comparable with the diffusion coefficient obtained through bulk analysis techniques, e.g., PITT.167

In Situ AFM Beyond LIBs. The Na-ion battery (NIB) is an important next generation energy storage system beyond LIB. Recently, in situ AFM was adapted to probe the sodiation process on both alloy- and intercalation-type NIB anodes. 151,152 For example, Lacey et al. studied Na⁺ intercalation on a planar MoS₂ anode with in situ AFM (Figure 5d-f). 151 A wrinkling effect at both the edge and basal planes was observed at the sodiated MoS₂ flake, which was attributed to the mechanical stress induced by intercalated Na+. The SEI formed in Na+ media was 2/3 times thinner than its Li⁺ counterpart in the same solution. Han et al. indicated a 420% initial volume expansion of Sn nanoparticle after the first sodiation (Figure 5g,h). 152 Compared to smaller Sn nanoparticles (70 nm), larger size Sn (240 nm) exhibited irreversible volume expansion-contraction during sodiation-desodiation cycles. A decrease in the Sn particle size led to a substantial enhancement of their cyclability and charge retention.

Future Directions. One of the recent developments is to couple AFM with SECM to obtain localized topography and electrochemical activity information. ¹⁶⁸ Zampardi et al. have previously demonstrated a AFM/SECM combined investigation of SEI at a glassy carbon surface. ¹⁶⁹ The SECM component can be successfully integrated to the AFM cantilever via diverse probe fabrication methods ^{170,171} or commercial products. ¹⁷² We believe the concurrent quantification of morphological, electrical, mechanical, and electrochemical maps using the coupled AFM/SECM technique can provide comprehensive understanding of surface and interface properties of diversified energy storage systems.

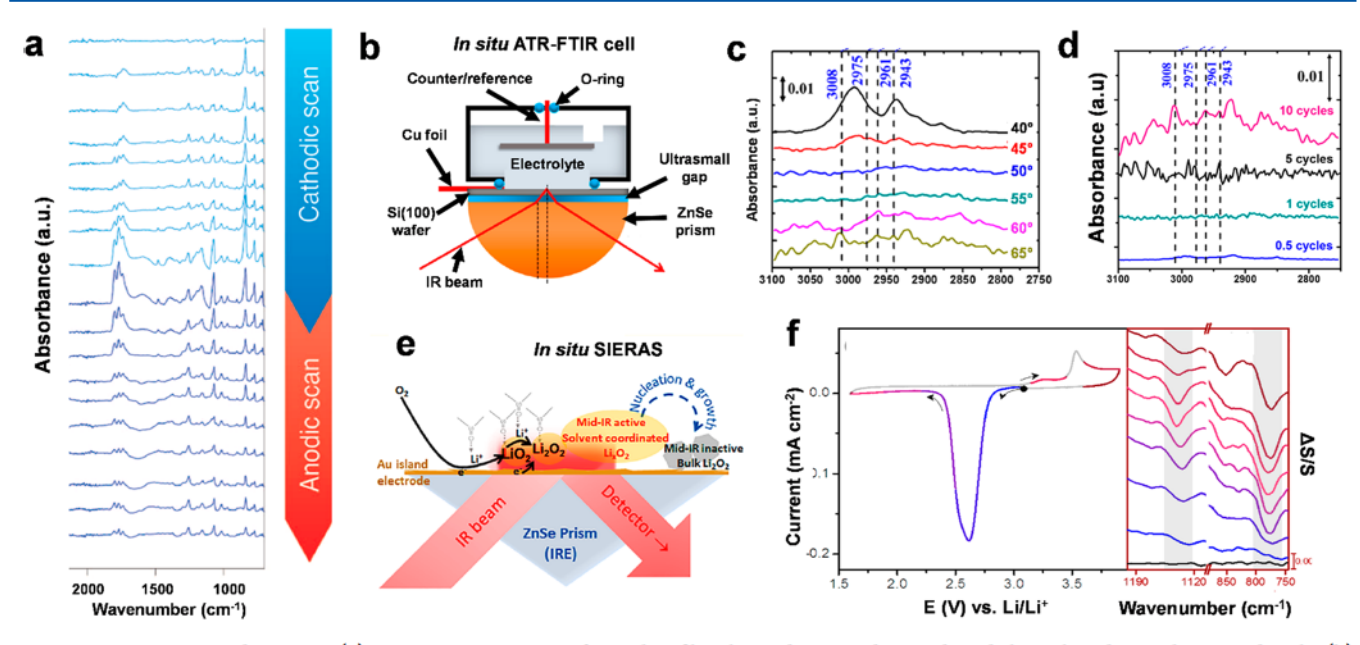


Figure 6. ATR-FT-IR and SEIRAS. (a) In situ FT-IR spectra of a Ni thin-film electrode in a carbonate-based electrolyte during the second cycle. (b) Schematic illustration of an in situ ATR-FT-IR spectra of lithiated silicon electrodes while the incidence angle varied between 40° (bulk electrode) and 65° (near-surface electrode region). (d) Near-surface ATR-FT-IR spectra of a Si(100) electrode in 1 M LiPF₆ electrolyte during cycling. The developing peaks are associated with lithium ethylene dicarbonate. (e) Schematic illustration of an in situ ATR-SEIRAS spectroelectrochemical cell. (f) CV of ORR/OER in dimethyl sulfoxide with 0.1 M lithium trifluoromethanesulfonate on a Au electrode and corresponding in situ SEIRA spectra. Part (a) reprinted with permission from J. Electrochem. Soc. 2018, 165, A1486—A1491 (ref 179). Copyright 2018, The Electrochemical Society. Parts (b—d) reproduced from Shi, F.; Ross, P. N.; Somorjai, G. A.; Komvopoulos, K. J. Phys. Chem. C 2017, 121, 14476—14483 (ref 180). Copyright 2017 American Chemical Society. Parts (e) and (f) reproduced from Vivek, J. P.; Berry, N. G.; Zou, J.; Nichols, R. J.; Hardwick, L. J. J. Phys. Chem. C 2017, 121, 19657—19667 (ref 181; https://pubs.acs.org/doi/abs/10.1021/acs.jpcc.7b06391). Published under Open Access by American Chemical Society, 2017.

■ ELECTROCHEMICAL COUPLED IN SITU CHARACTERIZATION

Electrochemistry alone cannot provide extensive knowledge about the atomic and molecular transformations underlying interfacial reactivity. Nonetheless, electrochemical techniques are amenable to coupling with powerful characterization techniques to monitor the interfacial changes upon electrochemical reactions in situ. In this section, we discuss in situ interfacial techniques including: Fourier transform infrared spectroscopy (FT-IR), Raman spectroscopy, sum frequency generation spectroscopy (SFG), X-ray absorption spectroscopy (XAS), X-ray photoelectron spectroscopy (XPS), X-ray reflectometry (XRR), and neutron reflectometry (NR), as well as transmission electron microscopy (TEM).

Fourier Transform Infrared Spectroscopy. FT-IR provides strong structural signatures¹⁷³ from the interaction between a beam of IR radiation (14300-20 cm⁻¹) and changes in the vibrational signatures of molecules. FT-IR methods provide identification of chemical species at electrified interfaces, including solvent molecule adsorption and intercalation, formation of electrode surface species, and breakdown products. 10 Improvements in the setup and methodologies have greatly simplified sample preparation and reproducibility for in situ interface studies. 10 The development of data processing methods including subtractively normalized interfacial FT-IR (SNIFT-IR), electrochemically modulated infrared spectroscopy (EMIRS), and potential modulation differential reflectance (PMDR) has improved analysis for sensitive and dynamic surface analysis. 174 There are numerous publications using in situ FT-IR to investigate the formation and stability of the SEI through detection of potential-dependent molecule orientation,

electrolyte reaction/breakdown potentials, SEI stability with cycling, and impact of additives. 10,173 Improved nanoscale spatial resolution for IR microscopy/mapping of battery interfaces can be achieved by multimodal methods including AFM and synchrotron light sources. 175,176 A development for in situ analysis of ionic transport at graphitic capacitor interfaces was also recently shown by Richey et al. 177,178 where they could quantify and track ionic liquid cations and anions during adsorption/desorption. However, in situ FT-IR studies on capacitive systems are not common. FT-IR sensitivity for identification and suitability for in situ analysis continue to make it highly desirable for interfaces.

The majority of publications on in situ electrochemical interfacial studies have relied on reflectance-based FT-IR methods. In these methods, reflected IR reveals information about surface processes in the cell. There are a few ways to acquire the reflected signal, distinguished into three categories. (1) Specular or external reflectance (SR), the most commonly applied method, is appropriate for smooth and reflective samples where a measurable signal returns from the interrogated sample surface. 10 (2) Attenuated total reflectance (ATR) is capable of measurements on opaque samples because it utilizes an internal reflection element that creates an evanescent wave that penetrates the sample/cell with a depth from hundreds of nanometers to micrometers (ca. 0.5 to 5 μ m). 182 (3) Diffuse reflectance (DR) avoids the reflection element and, instead, uses diffuse, or multiple, reflections from the sample and is suited for rough samples. However, DR has mostly been applied for ex situ samples.183

These methods have been highly successful at detecting a large variety of SEI species in an in situ manner¹⁰ revealing the extensive applicability for understanding interfacial elements

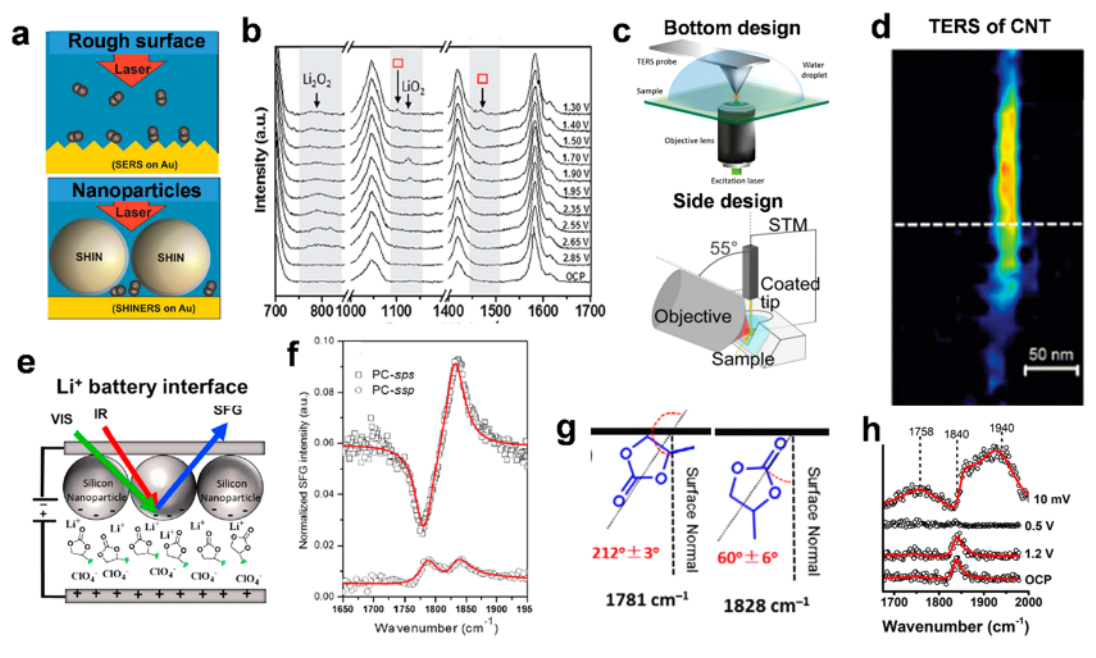


Figure 7. Raman and SFG spectroscopy. (a) Substrate designs for acquiring a SERS response. (b) In situ electrochemical Raman spectra with shell isolated nanoparticles (SHINs) of O₂ saturated 0.5 M LiClO₄ in dimethyl sulfoxide on graphite. (c) Designs for bottom and side TERS analysis. (d) TERS image of a SWCNT in water. (e) Schematic illustration of the electrode interface during in situ SFG. (f) SFG spectra observed on a carbon/PC interface with different polarization methods and fittings (red lines). (g) Derived schematic PC adsorption geometry at a carbon surface. (h) SFG spectra on a nanoparticle-based Si electrode as a function of potential in an EC-based electrolyte. Part (a) reproduced from Galloway, T. A.; Hardwick, L. J. J. Phys. Chem. Lett. 2016, 7, 2119–2124 (ref 193; https://pubs.acs.org/doi/abs/10.1021/acs.jpclett.6b00730). Published under Open Access by American Chemical Society, 2016. Part (b) reproduced from Galloway, T. A.; Cabo-Fernandez, L.; Aldous, I. M.; Braga, F.; Hardwick, L. J. Faraday Discuss. 2017, 205, 469–490 (ref 194). Published under Open Access by Royal Society of Chemistry, 2017. Parts (c) and (d) reproduced from Kumar, N.; Su, W.; Veselý, M.; Weckhuysen, B. M.; Pollard, A. J.; Wain, A. J. Nanoscale 2018, 10, 1815–1824 (ref 195), with permission of the Royal Society of Chemistry, 2018. Part (c) bottom figure reproduced from Martin Sabanés, N.; Driessen, L. M. A.; Domke, K. F. Anal. Chem. 2016, 88, 7108–7114 (ref 196; https://pubs.acs.org/doi/abs/10.1021/acs.analchem.6b01080). Published under Open Access by American Chemical Society, 2016. Parts (e) and (h) reproduced from Olson, J. Z.; Johansson, P. K.; Castner, D. G.; Schlenker, C. W. Chem. Mater. 2018, 30, 1239–1248 (ref 197). Copyright 2018 American Chemical Society. Parts (f) and (g) reprinted from Adsorption of organic carbonate solvents on a carbon surface probed by sum frequency generation (SFG) vibrational spectroscopy, Peng, Q.; Liu, H.; Ye, S. J. Electroanal. Chem. 2017, 800, 134–143 (ref 198), Copyright 2017 with p

during energy storage processes. Here, we try to deviate from some of the other most recent reviews discussing in situ IR methods for energy storage ^{10,173} to the most recent applications and developments, including those for new LIB systems, other metal-ion batteries, and metal—oxygen batteries.

Evaluation of the SEI. Recently, Kuwata and co-workers used ATR-FT-IR and SNIFT-IR to explore SEI formation and cycling performance (Figure 6a) on a Bi intermetallic electrode in different electrolytes. 179 Their methods followed suit to many previous studies 10 tracking species at the SEI. They found that traditional carbonate-based electrolytes resulted in capacity fade during the first few cycles and formation of decomposed electrolyte as identified by the negative peaks at 1101 and 916 cm⁻¹ and other decomposition products (Figure 6a). In contrast, the intermetallic anode performed better in an alternative electrolyte containing LiBH4 in tetrahydrofuran where the spectra were stable with cycling. Shi et al. also used ATR-FT-IR for evaluating SEI precursors at a Si electrode surface. 180 They provided an innovative setup where adjustments in the IR incidence angle (Figure 6b) led to changes in penetration depth helping to distinguish the interface from the bulk phases (Figure 6c). They were able to track the initial carbonate formation during the first half cycle and subsequent formation of Li-carbonate species after further cycling (Figure 6d). A few groups have also been successful using in situ DRIFT analysis on Si¹⁸⁴ and Ni- and Li-rich metal oxides. 185-187 IR-

based analysis continues to be highly relevant for tracking the interface changes and stability in LIB technologies as new materials, improved methodologies, and instrumentation are explored.

Application for Beyond LIBs. IR methods have also found applications for batteries beyond the LIB. For instance, Vivek et al. used in situ attenuated total reflectance surface enhanced infrared absorption spectroscopy (ATR SEIRAS) to detect metastable, solvated, and surface adsorbed species for metaloxygen batteries (Figure 6e,f). 181,188 ATR SEIRAS utilizes surface enhancement methods (e.g., nanoparticle assemblies), as shown in Figure 6e, to improve the FT-IR signal of molecules at an electrified interface (within 5 nm of the electrode). 189 With conventional IR techniques, it is difficult to detect the oxygenoxygen stretching bands of superoxide species, greatly limiting their application for cathodes in metal-oxygen batteries. Vivek and co-workers showed the SEIRAS method was able to detect some of these species during cyclic voltammetry at the substrate (Figure 6f) and could distinguish between different discharge pathways. 181 In another recent study, degradation of an ionic liquid, N-butyl-N-methylpyrrolidinium bis-(trifluoromethanesulfonyl) amide-TFSI or PYR14TFSI, for Li-air batteries was evaluated on a Au cathode with ATR-FT-IR. PYR₁₄TFSI was stable until a charging voltage beyond 4.3 V, where the ${\rm PYR_{14}}^+$ cation started to decompose and the anion remained stable. ¹⁹⁰ Likewise, in situ FT-IR methods are finding

application for SEI studies in alternative metal-ion batteries (e.g., Mg^{2+} , Na^+ , K^+). The versatility of this method is clearly applicable for understanding the SEI formation and evolution in a wide selection of energy storage systems.

Limitations and Future Directions. In spite of the broad application and sensitivity of IR-based methods, there are still limitations for evaluating interfaces relevant to energy storage. The SEI is typically a thin surface layer that may have components with weak vibration signals. Some inorganic compounds and large molecules with similar moieties remain elusive, 10,173 and the variability in signal intensities for certain moieties makes quantitative analysis difficult. Further, the composition of the SEI is often heterogeneous; thus, analysis of various sites to understand the significance of results is compromised by spatial and depth resolution. To date, there have been very limited studies on energy storage systems that provide localized information or mapping 192 and no published work containing in situ mapping. Often, IR methods have been limited to micrometer resolution (>10 μ m) due to the wavelength used and associated diffraction limit. Now, improved imaging technology through combination with AFM and IR sources of higher brightness (e.g., synchrotron) provides submicrometer resolution down to 20 nm. 175,176 In the near future, we expect to see in situ FT-IR mapping of the SEI as these techniques continue to develop.

Raman Spectroscopy. Raman spectroscopy provides complementary information to FT-IR of the molecular species within a sample. In Raman, monochromatic light (e.g., laser) interacts with molecular vibrations, or other excitations, resulting in a detectable energy shift of the scattered light. The laser, in the visible, near IR, or near UV, is chosen on the basis of the nature of the sample and its associated molecular excitation efficiencies, fluorescence, and heat adsorption. 10 As with FT-IR methods, the Raman shift provides a means for structural identification and tracking during electrochemical processes and continues to be applied extensively for in situ battery analysis. In situ Raman measurements are mainly applied for tracking phase change of electrode materials, 10,173,199 including next generation battery materials. 200-203 However, these typical Raman techniques provide little information about the processes occurring at the electrochemical interface. They are generally unable to detect the dynamic surface species at the SEI and CEI interfaces due to the relative thinness of such interfaces and low analyte concentrations. The interface species become observable through signal enhancing methods including surfaceenhanced and tip-enhanced Raman spectroscopies 205 (SERS and TERS, respectively) or when processes are confined to ultrathin interfaces. 23,116

Surface-Enhanced Raman Spectroscopy. SERS can improve the Raman signal by several orders of magnitude (10⁶–10¹¹) through incorporating nanoparticles, ¹⁰ often noble metals, onto the substrate surface or through patterning/roughening as shown in Figure 7a.²⁰⁶ The interactions of the laser with the electron clouds of the nanoscale structures results in an enhanced electromagnetic field at the surface. In situ SERS is especially popular for analysis of metal—oxygen battery interfaces where it can detect key intermediates including superoxide species. ^{194,206–208} A major development in SERS is the use of shell isolated nanoparticle-enhanced Raman spectroscopy, or SHINERS, with core—shell nanoparticles (SHINS) containing a SERS-active metallic core and a nanometer-thick insulating shell (Figure 7a, bottom). This structure minimizes contamination and interference by the SERS material and allows

Raman studies on a wider range of substrates. ²⁰⁹ Galloway et al. recently used SHINERS to study intermediates formed during ORR on a range of metallic, carbon-based, and semiconducting electrode materials that could not be studied with traditional SERS methods (Figure 7b). ^{193,194} New electrode and composite materials for LIB are also being explored with SHINERS. ²⁰⁹ In spite of the major developments in SERS, the signal is still limited to the space very near particular regions of the SERS or SHINERS nanostructures. This can complicate analysis and interpretation of the resulting measurements and may be troublesome when considering incorporation of mapping where the distribution of the nanostructures may not be homogeneous.

Limitation and Future Directions. There are a few experimental limitations with Raman including its application to only Raman-active species and possible degradation of some SEI components due to laser damage. The most notable drawback of in situ Raman studies on battery material interfaces is that it does not typically acquire localized information. It is common to acquire the measurement at a single site, although heterogeneities exist across most materials and interfaces. The use of Raman mapping and microscopy is quite common but rarely together with SERS. Recently, TERS is emerging for nanoscale measurements at different locations on an electrode surface.²¹⁰ TERS accesses localized chemical information through coupling the Raman measurements with nanoscale resolution scanning probe microscopy, e.g., AFM or STM. Cells for both bottom and side illumination have been developed (Figure 7c) and applied for electrochemical systems. 195,196 However, implementation of TERS for energy storage is quite rare because of difficulties working in a liquid electrolyte and maintaining optical coupling between the tip and laser. 195,211 We highlight the work by Kumar et al., who used TERS with AFM for Raman mapping of single carbon nanotubes (CNTs) in aqueous conditions (Figure 7d). 195 They utilized the G peak from the carbon in the CNT for mapping a sub-50 nm diameter wire. A similar report utilized TERS for high resolution mapping of graphene oxide flakes.²¹² It is apparent that Raman spectroscopy is excellent for evaluating/tracking and even mapping phase change of electrode materials during intercalation, conversion, and alloying reactions. However, there is still great opportunity in exploring the SEI with Raman mapping methodologies including TERS.

Sum Frequency Generation Spectroscopy. SFG is becoming more popular for interface analysis because of its simplicity and wide applicability for different interfaces. SFG provides information about surface adsorbates and their interfacial structures, which guide and impact the SEI formation mechanism. SFG is a nonlinear laser spectroscopy that involves two laser beams interacting to provide information about developing surfaces/interfaces (Figure 7e). Simultaneous interaction with both beams leads to second-order molecular responses that provide complementary information to that of IR and Raman. SFG is a highly surface-sensitive and -selective technique that can acquire molecular-level structural information at an electrified interface. 198 However, its development for such applications is very recent compared to other vibrational techniques. For further details on using SFG and analysis, we refer the reader to a few reviews covering its general application. 213,214

Tracking Molecular Orientation and Breakdown. Recently, SFG has been used for battery analysis to determine solvent molecule orientation at cathode and carbon-based interfaces. Peng and co-workers showed the use of polarized SFG

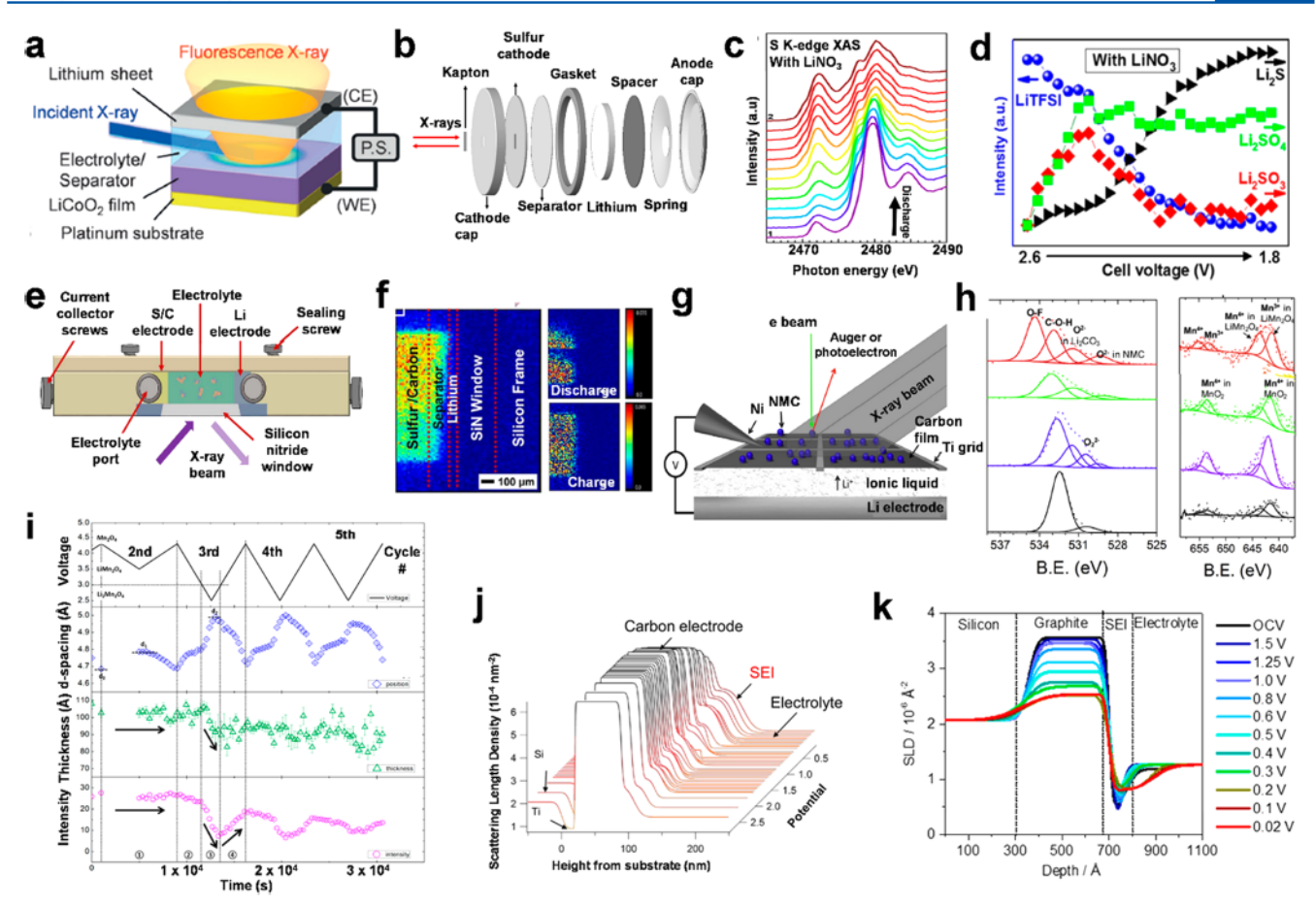


Figure 8. X-ray methods for evaluating interfaces in energy storage. (a) A spectroelectrochemical cell for in situ TRF-XAS measurements. (b) Schematic illustration of a coin cell design for operando XAS studies. (c) Operando S K-edge XAS spectra of a Li-S cell and (d) changes of different sulfur species during the 1st discharge process with a LiNO3 additive. (e) Top view of a cross-sectional cell design used for X-ray spectromicroscopy. (f) X-ray fluorescence map of a Li-S battery with battery stack components outlined (left) and mapping of Li₂S₈ species during the end of the first discharge (top) and charge (bottom) processes. (g) Schematic of an electrochemical cell for in situ XPS and in situ AES with solid electrolytes. (h) High resolution XPS scans for O 1s (left) and Mn 2p (right) on a Li[Ni_{1/3}Mn_{1/3}Co_{1/3}]O₂ cathode while charging. (i) Time sequence of the Li_xMn₂O₄ $(0 \le x \le 2)$ thin-film parameters with the associated voltage (top) including the LMO film thickness (middle) and the integrated intensity of the LMO (111) Bragg peak (bottom). (j) Scattering length density from NR measurements on a developing SEI at a carbon electrode. (k) Modeled NR scattering length density (SLD) profile during formation of SEI on carbon in a LiPF6 electrolyte. Part (a) reproduced from First In Situ Observation of the LiCoO2 Electrode/Electrolyte Interface by Total Reflection X-ray Absorption Spectroscopy, Takamatsu, D.; Koyama, Y.; Orikasa, Y.; Mori, S.; Nakatsutsumi, T.; Hirano, T.; Tanida, H.; Arai, H.; Uchimoto, Y.; Ogumi, Z. Angew. Chem., Int. Ed. 2012, 51, 11597-11601 (ref 222). Copyright 2012 Wiley. Parts (b-e) reprinted from The synergetic interaction between LiNO3 and lithium polysulfides for suppressing shuttle effect of lithium-sulfur batteries, Zhang, L.; Ling, M.; Feng, J.; Mai, L.; Liu, G.; Guo, J. Energy Storage Mater 2018, 11, 24-29 (ref 223), Copyright 2018 with permission from Elsevier. Part (f) reproduced from Miller, E. C.; Kasse, R. M.; Heath, K. N.; Perdue, B. R.; Toney, M. F. J. Electrochem. Soc. 2018, 165, A6043-A6050 (ref 224). Published under Open Access by the Electrochemical Society, 2018. Parts (g) and (h) reprinted from Surface redox on Li[Ni_{1/3}Mn_{1/3}Co_{1/3}]O₂ characterized by in situ X-ray photoelectron spectroscopy and in situ Auger electron spectroscopy, Tang, C.-Y.; Feng, L.; Haasch, R. T.; Dillon, S. J. Electrochim. Acta 2018, 277, 197-204 (ref 225), Copyright 2018 with permission from Elsevier. Part (i) reproduced from Chen, X.; Vörös, M.; Garcia, J. C.; Fister, T. T.; Buchholz, D. B.; Franklin, J.; Du, Y.; Droubay, T. C.; Feng, Z.; Iddir, H.; Curtiss, L. A.; Bedzyk, M. J.; Fenter, P. ACS Appl. Energy Mater. 2018, 1, 2526-2535 (ref 226). Copyright 2018 American Chemical Society. Part (j) reproduced from Kawaura, H.; Harada, M.; Kondo, Y.; Kondo, H.; Suganuma, Y.; Takahashi, N.; Sugiyama, J.; Seno, Y.; Yamada, N. L. ACS Appl. Mater. Interfaces 2016, 8, 9540-9544 (ref 227). Copyright 2016 American Chemical Society. Part (k) reproduced from Steinhauer, M.; Stich, M.; Kurniawan, M.; Seidlhofer, B.-K.; Trapp, M.; Bund, A.; Wagner, N.; Friedrich, K. A. ACS Appl. Mater. Interfaces 2017, 9, 35794-35801 (ref 228). Copyright 2017 American Chemical Society.

methods on LiCoO₂¹⁹⁸ for analyzing organic carbonate solvent molecule orientation at a carbon electrode. In their study, they evaluated the solvent species PC and DEC as well as additives. As exemplified with their data on PC (Figure 7f), two peaks were observed at 1782 and 1830 cm⁻¹ indicating two species with a phase difference near 180° (Figure 7g) for both polarization modes. ¹⁹⁸ In this fashion, they could estimate the bond angle normal to the surface for the phases of the two solvents and the surface coverage. The different polarization modes are useful to assign unclear vibrational modes in IR or Raman spectra and for

interpretation of the SFG spectral assignments since their signal intensities are dependent on the polarization. 213 Peng et al. 198 went on to study various solvent mixtures and the impact of additives. Through their methods, they could clearly observe preferential adsorption by certain species. Unfortunately, no bias was applied in this study.

Other groups have used SFG to monitor electrochemical reduction of solvent species. Recently, Olson et al. used operando SFG spectroscopy to monitor electrochemical reduction of LiClO₄/EC and LiClO₄/FEC at Si nanoparticle

electrodes. 197 SFG results from EC reduction indicated a liberation of oligomeric products that are soluble in the electrolyte solution and subsequent polymerized species at higher charge densities (Figure 7h). They clearly observed a decrease of the intact EC solvent (peak at 1840 cm⁻¹) upon moving from 1.2 to 0.5 V indicating its electrolysis but did not observe peaks associated with EC-based polymers or common SEI components. They interpreted this as soluble, EC-oligomer formation. However, moving to lower potentials resulted in polymer formation as indicated by the broad peak at 1758 cm⁻¹, while the EC solvent peak remained diminished and peaks associated with the SEI did not develop. For cycling in EC, they only observed the solvent peak. They interpreted their results as a lack of ordered SEI at the surface and solubilization of the formed polymeric species, agreeing with the capacity loss observed in the electrochemical measurements. In contrast, the FEC generated detectable Li₂CO₃ and CO species in the SFG, improved capacity retention, and suppressed soluble moieties.

Advantages and Limitations. The in situ application of SFG is proving to be highly useful for acquiring surface-sensitive, molecular-level information at interfaces relevant to energy storage. SFG can help guide our understanding of how the solvent molecules approach the electrode surface, their orientation during electrochemical processes, their degradation, and their interaction with other species during interface formation. This molecular level interfacial information may be very important for stable SEI formation and for understanding how its manipulation directly impacts material properties and lifespan. However, this technique is still developing and can require tedious analysis. It also currently suffers from issues with local heating and insensitivity to the SEI thickness. As with the other vibrational spectroscopies, SFG mapping is highly desirable but has yet to be applied for surface species in energy storage interfaces. ^{219,220}

X-ray Absorption Spectroscopy. XAS involves the tuning of photon energy, within the X-ray range, to excite core electrons of the different elemental components of the sample to provide insight into atomic structure. XAS is a versatile tool where fast, element specific, and sensitive (10–100 particles per mol) analyses can be applied to amorphous, small nanoparticles, and different phases (e.g., liquid, gas) in a sample. There are two main regions of interest within the XAS spectrum: X-ray absorption near-edge structure (XANES) and extended X-ray absorption fine structure (EXAFS). These regions complement one another to provide information on electronic transitions, site symmetries, oxidation state, coordination numbers, bond lengths, and chemical identity of the nearest

Surface Structure and Speciation Analysis. Recently, in situ XAS experiments have focused on noncrystalline species and monitoring phase changes during cycling to confirm their reversibility. ^{229–231} Metal dissolution and deposition has also been studied. ²³² Mapping of the lithiated and unlithiated species has allowed localized in situ monitoring of the intercalation process. ^{233,234} However, most studies are not extensively focused on the interface. In order to effectively extract information about the interfacial phenomena, specific techniques like total-reflection fluorescence XAS (TRF-XAS) are required.

TRF-XAS involves focusing the X-ray beam to the surface at a particular angle and collecting the fluorescence obtained under total reflection (Figure 8a). 222 Most of the in situ XAS work for battery analysis has been conducted by Takamatsu and

associates, who evaluated the metal species at the electrode surface as an indicator of the SEI evolution. ^{235–237} In one of their recent works, they monitored the surface and bulk processes of a LiCoO₂ electrode in EC/DEC and with the additive VC. ²³⁵ They observed improved ion movement at the electrode surface when VC was present. In situ XANES allowed tracking of electronic states and their transitions during electrochemical processes. They have also developed a setup that allowed fluctuation in penetration of the beam for acquiring better depth resolution. ²³⁶ By collecting emitted fluorescence signals at a 2D pixel array detector, they acquired a depth resolution of 3 nm. ²³⁵ Though these methods have proven to be powerful for identifying interfacial species, there have been minimal follow-up reports.

In other studies, the employment of unique cell designs provides an alternative for collecting information about the solvent and electrode surface in comparison to the commonly used coin cells. In a recent work by Zhang et al., the interaction between a LiNO3 additive and its impact on the SEI formation process was explored using in situ XAS. 223 To avoid interference from their sulfur cathode, they made a hole in its center that allowed the beam to pass through (Figure 8b) and interact better with the electrolyte and lithium anode. By tracking various peaks during the discharge process (Figure 8c,d), they found that LiNO₃ and intermediate polysulfides formed leading to the formation of a stable SEI layer. Though they were not directly focused on the surface, the insolubility of the observed species led to their assignment as part of the SEI. Miller et al. recently used a cross-sectional cell design (Figure 8e) that simultaneously allowed them to map different regions of the battery cell (Figure 8f, left).²²⁴ During operando measurements, they tracked multiple species enabling mapping of the species distribution as shown for Li₂S_X species during charge and discharge (Figure 8f, right), albeit with low resolution. Alternatively, the employment of transmission X-ray microscopy (TXM) can provide a means to map species as they deposit within a working battery and at their interfaces. 238,239 These methods are also limited to micrometer scale resolution.

Limitations and Future Directions. XAS provides a mechanistic approach toward the study of interfacial reactions but can involve difficult analysis depending on the number of species in the system. Specifically, TRF-XAS has great potential for understanding processes at energy storage interfaces. Its high surface sensitivity and capability for depth profiling make it highly desirable. Mapping methods based on XAS also look promising, though groups need to move toward an understanding and sensitivity beyond phase change or intercalation/deintercalation.

X-ray Photoelectron Spectroscopy. XPS is used to analyze the elemental composition of a surface of different types of materials by using photons in the X-ray range that cause core electrons to be emitted from the material. Specific methods such as hard X-ray photoelectron spectroscopy (HAXPES) provide a means to study the interface and bulk material beneath simultaneously. Unfortunately, in situ analysis of battery materials with XPS has not been developed for liquid cells. Instead, XPS has been used extensively for studying the SEI ex situ and for in situ measurements on solid electrolytes and their solid—solid interfaces. 10,240—242

Oxidation State and Species Identification. Only recently, the first presence of a liquid electrolyte (LiClO₄ in PC) during XPS was realized by using a low pressure N₂ environment in the analysis chamber and by avoiding ultrahigh vacuum during

transfer. 243 This report represented a major step toward operando solid/liquid interface studies using liquid electrolytes. However, since that report, the methods have not improved for in situ liquid electrolyte measurements. This technique frequently relies on an ultrahigh vacuum which makes in situ analysis difficult, though a few groups have employed ionic liquids as an alternative. 22.5,244 In recent work by Tang and associates, an open cell (Figure 8g) allowed them to take in situ XPS and auger electron spectroscopic (AES) measurements on a LIB cathode. 22.5 AES is similar to XPS except that the formation mechanism of the ejected electron is different. Through XPS and AES, they were able to identify a wide variety of species and oxidation states for the electrode components (Figure 8h).

Current Limitations. In spite of the recent developments, there are still several experimental difficulties that need to be overcome to make in situ XPS more practical and widely applicable for analysis in energy storage. The largest step for XPS finding broader application to energy storage systems is further in situ development for liquid electrolytes. The elemental information gained with XPS is highly desirable for in situ studies. For example, a recent manuscript described a methodology for simultaneously obtaining CV data with XPS on a ferrocene-terminated self-assembled monolayer, successfully characterizing the impact of oxidation state. Aside, there are a few other issues associated with XPS. The predominant insulating materials in the SEI can lead to a charging problem, and secondary reactions and artifacts may also occur.

X-ray Reflectometry. XRR is a surface-sensitive analytical technique that characterizes film formation at surfaces and evaluates film thickness and roughness on thin films and multilayers. In XRR, an X-ray beam is reflected on the basis of Fresnel's Law of reflection from a flat surface at a grazing angle to prevent beam penetration; the intensity of the reflected X-rays is collected. XRR is compatible with crystalline and amorphous samples and can provide detailed structural information over optical measurements. Overall, the developments and applications of XRR to the energy storage interfaces are recent, but most have focused on evaluating dendrite growth or reversible/ irreversible film formation on interfaces including some SEI studies. 10,226,246,247 Typically, XRR is only able to track changes in the SEI and/or material thickness during operation, and structural components are not specifically identified. In a recent work by Chen et al., low-angle and crystal truncation rods (CTR) XRR measurements were performed in operando for tracking Mn reorganization (phase change) and changes in material thickness of a thin lithium manganate (LMO) electrode film. 226 As shown in Figure 8i, changes in the LMO Bragg peak (tracked via the CTR) provide insight into the LMO thickness during operation and reversibility.

Neutron Reflectometry. NR utilizes a collimated neutron beam at a grazing angle to the surface. NR has better penetration depth (several centimeters) and resolution between the interfaces and is better suited for detecting lighter elements (e.g., Li, O) compared with XRR. It can be used to detect the SEI formation, lithiation, and plating processes in situ. ²²⁷, ²²⁸, ²⁴⁸, ²⁴⁹ Recently, Kawaura et al. were able to directly observe the SEI growth process and subsequent intercalation using time-slicing NR on a 70 nm carbon film (Figure 8j). ²²⁷ Through fitting, they were able to differentiate changes in different layers, including the SEI, of their model battery. However, they were not able to clarify the actual chemical components. Another report using NR on a carbon film by Steinhauer et al. ²²⁸ also showed the

ability to decouple various layers of the operating cell. As shown in their NR and subsequent fitting (Figure 8k), they were able to clearly resolve changes in thickness of the carbon electrode and SEI. Further, they could observe the Li population increase at the surface during operation.

One major drawback for XRR and NR is the requirement for flat electrode surfaces to produce a strong signal. These techniques typically lack the ability or development to identify compositional, morphological, and specific reactions at the interfaces. NR provides some benefits over XRR such as sensitivity for light elements, but NR also requires properly designed solvent (e.g., deuterated or mixed solvent) to enhance the contrast and involves longer analysis times. Producing and handling neutrons outside of a particle accelerator is difficult, and there are fewer neutron facilities compared with synchrotrons. Ultimately, both techniques are promising for tracking changes in the EEI thickness and composition.

Transmission Electron Microscopy. TEM is an imaging method that uses high-energy electrons to acquire angstrom (Å) level resolution across a sample. 10,250 Analysis at this scale helps in visualizing the evolution of the surface morphology at the interface where changes can vary from subnanometers to tens of nanometers. TEM can collect high-resolution phase information at different points and is compatible with nanometer-sized particles. 251,252 During TEM, electrons undergo multiple phenomena including penetration into the sample, absorption, and diffraction. The diffracted electrons result in a pattern of spots and rings indicative of the crystallographic phases present. TEM is also capable of elemental composition analysis and distribution through energy dispersive X-ray analysis (EDX or EDS). Alternatively, measurements of the absorbed electron energy through electron energy loss spectroscopy (EELS) enable determination of the oxidation states. Overall, TEM provides a near complete material analysis with atomic level information, bulk morphology, and elemental composition.1 For energy storage, most in situ TEM reports have focused on phase transformation, changes in morphology during the lithiation process, direction/face preferences for intercalation, and interfacial changes during lithiation. 250,253 Throughout these studies, both TEM cells for open (all solid batteries, solidstate SEI) and closed (liquid) environments were used for in situ/in operando studies.

Solid-Liquid Interface. Closed, or liquid, TEM cells utilize a sealed electrochemical setup that can withstand the vacuum environment but provides electron penetration via an electron transparent window (e.g., SiN). This makes TEM compatible with most common liquid electrolytes of lithium-ion batteries for in situ and/or in operando conditions. Most closed TEM electrochemical cells involve a micrometer-sized assembly on top of a silicon chip and continuous flow of the electrolyte via nanochannels (Figure 9a).²⁵⁴ Recently, Lutz et al. used fast imaging TEM on a Na-O2 microbattery in a liquid cell to visualize the mechanism of NaO2 nucleation and growth. 254 They were able to distinctly observe changes in the interface (Figure 9b) and along with ex situ measurements could distinguish multiple layers and an amorphous, organic outer shell. They determined the cube growth followed a solutionprecipitation mechanism. Another liquid cell, the graphene liquid cell (GLC), uses two graphene sheets to trap energy materials and electrolyte (Figure 9c). Within this cell, Yuk et al. used the electron beam to stimulate chemical lithiation into Si nanoparticles while it was monitored by TEM. 257 They could observe dimensional changes and phase preference for the

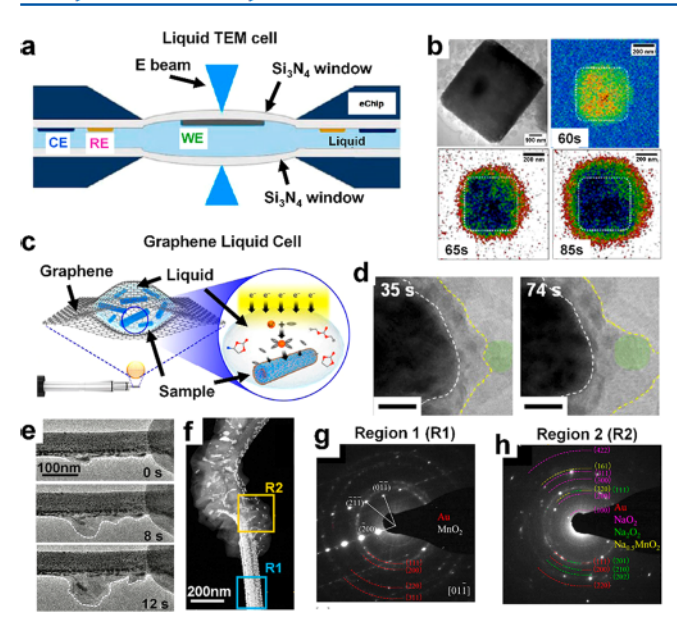


Figure 9. Transmission electron microscopy of energy materials. (a) A liquid TEM cell design, utilizing an electron-transparent Si3N4 window and flowable electrolyte. (b) High-resolution TEM image of NaO2 cube at the end of discharge (top-left). Operando (top-right and bottom) evolution of a growing NaO2 cube. (c) Graphene liquid cell design for TEM, utilizing two sheets of graphene to trap an electrolyte solution and material of interest. (d) High magnification in situ TEM of a SnO₂ nanotube during lithiation showing the formation process and changes in a thick amorphous layer (white and yellow outlines). (e) Morphology changes and growth of discharge products nucleating at Au clusters on a Au/MnO₂ air cathode while discharging. Morphology (f) and phase characterization of the deposits on a Au/MnO2 NW air cathode after discharge with the electron diffraction patterns (g, h) collected at different regions (yellow and blue squares). Parts (a) and (b) reproduced from Lutz, L.; Dachraoui, W.; Demortière, A.; Johnson, L. R.; Bruce, P. G.; Grimaud, A.; Tarascon, J.-M. Nano Lett. 2018, 18, 1280-1289 (ref 254). Copyright 2018 American Chemical Society. Parts (c) and (d) reprinted from Growth dynamics of solid electrolyte interphase layer on SnO2 nanotubes realized by graphene liquid cell electron microscopy, Cheong, J. Y.; Chang, J. H.; Seo, H. K.; Yuk, J. M.; Shin, J. W.; Lee, J. Y.; Kim, I.-D. Nano Energy 2016, 25, 154-160. (ref 255), Copyright 2016 with permission from Elsevier. Parts (e-h) reprinted from In situ imaging electrocatalysis in a Na-O2 battery with Au-coated MnO2 nanowires air cathode, Liu, Q.; Geng, L.; Yang, T.; Tang, Y.; Jia, P.; Li, Y.; Li, H.; Shen, T.; Zhang, L.; Huang, J. Energy Storage Mater. 2018, in press (ref 251), Copyright 2018 with permission from Elsevier.

lithiation process. A more recent work used the same concept and cell to evaluate SnO_2 nanotubes. ²⁵⁵ In this work, they could clearly observe fluctuations in decomposed electrolyte at the interface (Figure 9d). Recent technical advances have focused on exploring the morphological impact of damage upon cycling on interfaces such as Si and Li anodes. ^{258,259} One relevant direction in these studies is the collection of electrochemical data from small structures and electrodes, enabling galvanostatic experiments at low applied currents for a more detailed understanding of the relationship between electrochemical performance and the qualities of the interrogated sample.

Solid—Solid Interface. Aside from liquid TEM studies, open cells under the typical conditions of high vacuum TEM are useful for studying solid—solid interfaces as in solid-state batteries and for viscous electrolytes (e.g., ionic liquids). Recent work investigating Na—O₂ battery materials in an open cell by Liu et al. showed transformation of the electrode material during

electrochemical reaction (Figure 9e). 251 Under the TEM resolution, the interfaces between materials could be realized over time clearly showing deposition and clustering of decomposition products (Figure 9e,f). They could also differentiate the species within different regions (Figure 9f–h), and additional EELS analysis provided further evaluation of the species present during operation.

Current Limitations. The main issue with TEM analysis is beam damage at the sample. Electron beams generate heat on interaction with matter that can decompose battery and SEI components. ^{10,250} Also, the beam can generate gaseous products with organic electrolytes as for the case of LiPF₆. Although it is possible, it still remains difficult to acquire quantitative electrochemistry in the electron microscope. ^{2,52} Further, the use of EELs is greatly disrupted by a liquid cell due to scattering from the liquid hindering quantitative analysis. Altogether, TEM has great potential, and there is even a proposal to use the beam damage as an analytical tool: through rational chemical perturbation with species generated by the electron beam, imaging of chemically driven, nanometer-scale dynamics can be acquired. ²⁶⁰

Aside from TEM, scanning electron microscopy, SEM, is also potentially useful for visualizing the changing SEI. However, the resolution for the microscope is typically poorer than TEM, and charging can be more problematic. The SEM also uses a high vacuum working environment, and typical battery electrolytes will interact with the electron beam. Thus, SEM has mostly been limited to carbon-based materials, solid electrolytes, or ionic liquids. Alternatively, inert sample transfer chambers have also been used for SEM measurements in between electrochemical perturbation. Work is still required to access measurements in organic liquid electrolytes.

■ FINAL REMARKS

We have reviewed the current developments of (coupled) electrochemical techniques and their applications to characterize energy storage interfacial properties in situ and across various spatial and temporal scales. We noticed that the majority of the research took place within the realm of lithium-ion batteries. Energy storage systems beyond Li-ion are significant emerging technologies, including sulfur and metal—air batteries, Na⁺ and K⁺ batteries, and multivalent aluminum and magnesium batteries, as well as redox flow batteries. Despite the differences in electrode material, electrolyte, and charge storage mechanism, energy storage systems share common limitations in electron and ion mobility within interfaces. Hence, we anticipate that the theory and instrumental progress developed for studies in LIB systems will be directly applicable to the analysis of new interfaces in the emerging energy storage systems.

Several interesting interfacial processes that are still under discovery are listed here for future attention. In LIB, the roles of electrode surface modification, artificial SEI, component leaching, and electrode morphological changes upon cycling need to be addressed. Further studies for beyond Li-ion systems include the proper surface conditioning of carbon-based materials for improved alkali-ion diffusion and intercalation for Na $^+$ and K $^+$ batteries. Moreover, improving surface coatings to prevent Li dendrite formation in Li-metal anodes, diminishing the polysulfide shuttle effects in the Li–S battery, and preventing the Li₂O₂ deposition at the electrode surface and/or promoting its cyclability in the Li–O₂ battery are necessary. We expect that, in the coming years, insightful studies exploring the chemistries of emerging systems such as other metal—air $^{26\,1,262}$ and redox

flow batteries ^{87,263–267} will gain prominence in the development of new analytical tools, including nanoelectrochemical approaches. ^{82,268} Fundamental knowledge of electrochemical interfaces obtained via novel analytical tools will play a key part in the future development of reliable, low-cost, and high-performance energy storage systems.

AUTHOR INFORMATION

Corresponding Author

*E-mail: joaquinr@illinois.edu. Phone: 217-300-7354.

ORCID

Jingshu Hui: 0000-0002-6987-4414

Kenneth Hernández-Burgos: 0000-0002-4644-784X Joaquín Rodríguez-López: 0000-0003-4346-4668

Notes

The authors declare no competing financial interest.

Biographies

Jingshu Hui finished her B.S. degree in College of Chemistry and Molecular Engineering at Peking University (China) in 2011. She completed her Ph.D. degree in the Department of Materials Science and Engineering at University of Illinois at Urbana—Champaign (USA) under the supervision of Prof. Joaquin Rodriguez-López in 2017. Her doctoral thesis was focused on electrochemical mechanisms in nanostructured graphitic and redox-active polymeric architectures. She is now continuing her research in the Rodriguez-López lab as a postdoctoral research associate. Her current work focuses on elucidating the (co)intercalation mechanism and surface modification effects in alkali-ion-based energy storage systems.

Zachary T. Gossage completed his B.S. degree in the Department of Biological Sciences at Western Illinois University (Macomb, IL, USA) in 2010 followed by his M.S. degree in the Department of Chemistry at the same university in 2014. He is currently a Ph.D. candidate in the Department of Chemistry at the University of Illinois at Urbana—Champaign. Under the supervision of Dr. Joaquin Rodríguez-López, his thesis work is focused on developing and utilizing electroanalytical methods for understanding current issues in energy storage including measurements on single particle battery materials, tracking alkalineions at functioning electrode—electrolyte interfaces, and developing new recovery methods for spent lead acid batteries.

Dipobrato Sarbapalli earned his bachelor's degree (B.Tech.) in Civil Engineering at National Institute of Technology, Tiruchirappalli (India) in 2015, followed by a master's degree (M.S.) in Civil Engineering at University of Illinois at Urbana—Champaign in 2018. His M.S. thesis under Prof. Paramita Mondal focused on understanding nucleation kinetics and reaction mechanisms of sustainable, alternative, aluminosilicate binder materials termed as geopolymers. Afterwards, he joined Prof. Joaquín Rodríguez-López's research group as a Ph.D. student and is currently working on the characterization of alkali-ion intercalation within graphene.

Kenneth Hernández-Burgos earned a bachelor's degree in chemistry from the University of Puerto Rico at Río Piedras (UPR-RP) in 2010. During his time at UPR-RP, he was a Minority Access for Research Careers fellow and worked under the supervision of Prof. Ana R. Guadalupe developing electrochemical biosensors. He earned his Ph.D. in the department of chemistry and chemical biology at Cornell University in Prof. Héctor D. Abruña's lab in which he worked on the design and characterization of organic electrode materials for electrical energy storage applications. As a Beckman postdoctoral fellow in the Rodriguez-López laboratory, he works in the design and electrochemical characterization of redox-active polymers.

Joaquín Rodríguez-López is an associate professor of chemistry at the University of Illinois. Originally from Mexico, he obtained a degree in chemistry from Tecnológico de Monterrey working under the supervision of Prof. Marcelo Videa. He then obtained a Ph.D. at the University of Texas at Austin with Prof. Allen J. Bard and did a postdoctoral stay with Prof. Héctor D. Abruña at Cornell University. His research program advances electrochemical characterization strategies and imaging methods for novel energy nanomaterials, and he is interested in new strategies for redox flow batteries and for ultrathin electrodes as proxy systems to interfaces.

■ ACKNOWLEDGMENTS

The authors gratefully acknowledge financial support from the National Science Foundation under grants NSF DMR 16-11268 and NSF CHE 17-09391. K.H.-B. gratefully acknowledges the Beckman Institute Postdoctoral Fellowship at the University of Illinois at Urbana—Champaign and the additional funding provided by the Arnold and Mabel Beckman Foundation.

REFERENCES

- (1) Jamtveit, B.; Meakin, P. In Growth, Dissolution and Pattern Formation in Geosystems; Springer: Dordrecht, 1999; p 291.
- (2) Hernández-Burgos, K.; Barton, Z. J.; Rodríguez-López, J. Chem. Mater. 2017, 29, 8918-8931.
- (3) Basic Research Needs for Next Generation Electrical Energy Storage; U.S. Department of Energy, Office of Science: Washington, DC, 2017.
- (4) Yu, X.; Manthiram, A. Energy Environ. Sci. 2018, 11, 527-543.
- (5) Nitta, N.; Wu, F.; Lee, J. T.; Yushin, G. Mater. Today 2015, 18, 252-264.
- (6) Gauthier, M.; Carney, T. J.; Grimaud, A.; Giordano, L.; Pour, N.; Chang, H.-H.; Fenning, D. P.; Lux, S. F.; Paschos, O.; Bauer, C.; Maglia, F.; Lupart, S.; Lamp, P.; Shao-Horn, Y. J. Phys. Chem. Lett. 2015, 6, 4653–4672.
- (7) Barton, Z. J.; Rodríguez-López, J. Anal. Bioanal. Chem. 2016, 408, 2707-2715.
- (8) Wu, Y.; Liu, N. Chem. 2018, 4, 438-465.
- (9) Yang, Y.; Liu, X.; Dai, Z.; Yuan, F.; Bando, Y.; Golberg, D.; Wang, X. Adv. Mater. 2017, 29, 1606922.
- (10) Tripathi, A. M.; Su, W.-N.; Hwang, B. J. Chem. Soc. Rev. 2018, 47, 736-851.
- (11) Elgrishi, N.; Rountree, K. J.; McCarthy, B. D.; Rountree, E. S.; Eisenhart, T. T.; Dempsey, J. L. J. Chem. Educ. 2018, 95, 197–206.
- (12) Orazem, M. E.; Tribollet, B. Electrochemical impedance spectroscopy, 1st ed.; John Wiley & Sons: Hoboken, NJ, 2008.
- (13) Levi, M. D.; Aurbach, D. Potentiostatic and Galvanostatic Intermittent Titration Techniques. *Charact. Mater.* 2012; DOI: 10.1002/0471266965.com125
- (14) Buttry, D. A.; Ward, M. D. Chem. Rev. 1992, 92, 1355-1379.
- (15) Talaie, E.; Bonnick, P.; Sun, X.; Pang, Q.; Liang, X.; Nazar, L. F. Chem. Mater. 2017, 29, 90–105.
- (16) Bard, A. J.; Faulkner, L. R. Electrochemical Methods: Fundamentals and Applications, 2nd ed.; John Wiley and Sons: New York, 2001.
- (17) Kissinger, P.; Heineman, W. R. Laboratory Techniques in Electroanalytical Chemistry, 2nd ed.; Marcel Dekker, Inc: New York, 1996.
- (18) Lei, T.; Xie, Y.; Wang, X.; Miao, S.; Xiong, J.; Yan, C. Small 2017, 13, 1701013.
- (19) Wu, H.-L.; Haasch, R. T.; Perdue, B. R.; Apblett, C. A.; Gewirth, A. A. J. Power Sources 2017, 369, 50-56.
- (20) Vogl, U. S.; Lux, S. F.; Das, P.; Weber, A.; Placke, T.; Kostecki, R.; Winter, M. J. Electrochem. Soc. 2015, 162, A2281—A2288.
- (21) Yoo, H. D.; Liang, Y.; Dong, H.; Lin, J.; Wang, H.; Liu, Y.; Ma, L.; Wu, T.; Li, Y.; Ru, Q.; Jing, Y.; An, Q.; Zhou, W.; Guo, J.; Lu, J.; Pantelides, S. T.; Qian, X.; Yao, Y. Nat. Commun. 2017, 8, 339.
- (22) Choudhury, S.; Tu, Z.; Stalin, S.; Vu, D.; Fawole, K.; Gunceler, D.; Sundararaman, R.; Archer, L. A. Angew. Chem., Int. Ed. 2017, 56, 13070–13077.

- (23) Hui, J.; Schorr, N. B.; Pakhira, S.; Qu, Z.; Mendoza-Cortes, J. L.; Rodríguez-López, J. J. Am. Chem. Soc. 2018, 140, 13599–13603.
- (24) Nicolau, B. G.; Petronico, A.; Letchworth-Weaver, K.; Ghadar, Y.; Haasch, R. T.; Soares, J. A. N. T.; Rooney, R. T.; Chan, M. K. Y.; Gewirth, A. A.; Nuzzo, R. G. Adv. Mater. Interfaces 2018, 5, 1701292.
- (25) Clancy, T. M.; Rohan, J. F. ChemElectroChem 2018, 5, 3273.
- (26) Friedl, J.; Stimming, U. Electrochim. Acta 2017, 227, 235-245.
- (27) Li, Y.; Yan, K.; Lee, H.-W.; Lu, Z.; Liu, N.; Cui, Y. Nat. Energy 2016, 1, 15029.
- (28) Fan, L.; Zhuang, H. L.; Gao, L.; Lu, Y.; Archer, L. A. J. Mater. Chem. A 2017, 5, 3483-3492.
- (29) Song, X.; Liu, T.; Amine, J.; Duan, Y.; Zheng, J.; Lin, Y.; Pan, F. Nano Energy 2017, 37, 90–97.
- (30) Yu, X.; Manthiram, A. Acc. Chem. Res. 2017, 50, 2653-2660.
- (31) Song, H.-Y.; Jeong, S.-K. J. Power Sources 2018, 373, 110-118.
- (32) Lu, D.; Tao, J.; Yan, P.; Henderson, W. A.; Li, Q.; Shao, Y.; Helm, M. L.; Borodin, O.; Graff, G. L.; Polzin, B.; Wang, C.-M.; Engelhard, M.; Zhang, J.-G.; De Yoreo, J. J.; Liu, J.; Xiao, J. *Nano Lett.* 2017, 17, 1602–1609.
- (33) Haregewoin, A. M.; Terborg, L.; Zhang, L.; Jurng, S.; Lucht, B. L.; Guo, J.; Ross, P. N.; Kostecki, R. *J. Power Sources* 2018, 376, 152–160.
- (34) Levi, M. D.; Aurbach, D. J. Phys. Chem. B 1997, 101, 4630-4640.
- (35) Hui, J.; Burgess, M.; Zhang, J.; Rodríguez-López, J. ACS Nano 2016, 10, 4248-4257.
- (36) Tu, Z.; Choudhury, S.; Zachman, M. J.; Wei, S.; Zhang, K.; Kourkoutis, L. F.; Archer, L. A. Nat. Energy 2018, 3, 310-316.
- (37) Yin, Y.-X.; Xin, S.; Guo, Y.-G.; Wan, L.-J. Angew. Chem., Int. Ed. 2013, 52, 13186–13200.
- (38) Huggins, R. A. Energy storage, 2nd ed.; Springer: New York, 2016.
- (39) Pan, H.; Chen, J.; Cao, R.; Murugesan, V.; Rajput, N. N.; Han, K. S.; Persson, K.; Estevez, L.; Engelhard, M. H.; Zhang, J.-G.; Mueller, K. T.; Cui, Y.; Shao, Y.; Liu, J. *Nat. Energy* 2017, 2, 813–820.
- (40) Schneider, A.; Janek, J.; Brezesinski, T. Phys. Chem. Chem. Phys. 2017, 19, 8349-8355.
- (41) Yang, Y.; Tang, D.-M.; Zhang, C.; Zhang, Y.; Liang, Q.; Chen, S.; Weng, Q.; Zhou, M.; Xue, Y.; Liu, J.; Wu, J.; Cui, Q. H.; Lian, C.; Hou, G.; Yuan, F.; Bando, Y.; Golberg, D.; Wang, X. *Energy Environ. Sci.* 2017, 10, 979–986.
- (42) Jin, Y.; Zhu, B.; Lu, Z.; Liu, N.; Zhu, J. Adv. Energy Mater. 2017, 7, 1700715.
- (43) Zhao, J.; Zhou, G.; Yan, K.; Xie, J.; Li, Y.; Liao, L.; Jin, Y.; Liu, K.; Hsu, P.-C.; Wang, J.; Cheng, H.-M.; Cui, Y. Nat. Nanotechnol. 2017, 12,
- (44) Sun, Y.; Zheng, G.; Seh, Z. W.; Liu, N.; Wang, S.; Sun, J.; Lee, H. R.; Cui, Y. Chem. 2016, 1, 287–297.
- (45) Schiele, A.; Breitung, B.; Hatsukade, T.; Berkes, B. B.; Hartmann, P.; Janek, J.; Brezesinski, T. ACS Energy Lett. 2017, 2, 2228-2233.
- (46) Zhao, W.; Zheng, G.; Lin, M.; Zhao, W.; Li, D.; Guan, X.; Ji, Y.; Ortiz, G. F.; Yang, Y. J. Power Sources 2018, 380, 149–157.
- (47) Kim, M. S.; Kim, M.-S.; Do, V.; Lim, Y. R.; Nah, In W.; Archer, L. A.; Cho, W. I. Nano Energy 2017, 41, 573-582.
- (48) Choi, S.; Jung, G.; Kim, J. E.; Kim, T.; Suh, K. S. Appl. Surf. Sci. 2018, 455, 367–372.
- (49) Kim, S. H.; Heo, S.; Mun, J.; Kim, G.; Baek, W. J.; Kim, Y. S.; Han, S.; Jung, H. J. Electrochem. Soc. 2017, 164, A2290—A2294.
- (50) Neudeck, S.; Walther, F.; Bergfeldt, T.; Suchomski, C.; Rohnke, M.; Hartmann, P.; Janek, J.; Brezesinski, T. ACS Appl. Mater. Interfaces 2018, 10, 20487–20498.
- (51) Liu, Q. Q.; Ma, L.; Du, C. Y.; Dahn, J. R. Electrochim. Acta 2018, 263, 237-248.
- (52) Kim, T.; Leyden, M. R.; Ono, L. K.; Qi, Y. Carbon 2018, 132, 678-690.
- (53) Barsukov, Y.; Macdonald, J. R. Electrochemical Impedance Spectroscopy. Charact. Mater. 2012; DOI: 10.1002/ 0471266965.com124
- (54) Liang, M.; Zhi, L. J. Mater. Chem. 2009, 19, 5871-5878.
- (55) Song, H.-K.; Lee, K. T.; Kim, M. G.; Nazar, L. F.; Cho, J. Adv. Funct. Mater. 2010, 20, 3818–3834.

- (56) Song, M.-K.; Park, S.; Alamgir, F. M.; Cho, J.; Liu, M. Mater. Sci. Eng., R 2011, 72, 203–252.
- (57) Roy, P.; Srivastava, S. K. J. Mater. Chem. A 2015, 3, 2454-2484.
- (58) Xu, Y.; Zhou, M.; Lei, Y. Adv. Energy Mater. 2016, 6, 1502514.
- (59) Lin, D.; Liu, Y.; Liang, Z.; Lee, H.-W.; Sun, J.; Wang, H.; Yan, K.; Xie, J.; Cui, Y. Nat. Nanotechnol. 2016, 11, 626.
- (60) Wang, J.; Wu, C.; Deng, Q.; Jiang, K.; Shang, L.; Hu, Z.; Chu, J. Nanoscale 2018, 10, 13140–13148.
- (61) Bin, H.; Yao, Z.; Zhu, S.; Zhu, C.; Pan, H.; Chen, Z.; Wolverton, C.; Zhang, D. J. Alloys Compd. 2017, 695, 1223–1230.
- (62) Jung, S.; Jung, H. Chem. Phys. Lett. 2018, 706, 189-195.
- (63) He, J.; Chen, Y.; Manthiram, A. Science 2018, 4, 36-43.
- (64) Bracamonte, M. V.; Primo, E. N.; Luque, G. L.; Venosta, L.; Bercoff, P. G.; Barraco, D. E. *Electrochim. Acta* 2017, 258, 192-199.
- (65) Choudhury, S.; Wei, S.; Ozhabes, Y.; Gunceler, D.; Zachman, M. J.; Tu, Z.; Shin, J. H.; Nath, P.; Agrawal, A.; Kourkoutis, L. F.; Arias, T. A.; Archer, L. A. *Nat. Commun.* 2017, 8, 898.
- (66) Morales-Ugarte, J. E.; Bolimowska, E.; Rouault, H.; Santos-Peña, J.; Santini, C. C.; Benayad, A. J. Phys. Chem. C 2018, 122, 18223—18230.
- (67) Huang, Q.-A.; Shen, Y.; Huang, Y.; Zhang, L.; Zhang, J. Electrochim. Acta 2016, 219, 751-765.
- (68) Ogihara, N.; Itou, Y.; Sasaki, T.; Takeuchi, Y. J. Phys. Chem. C 2015, 119, 4612-4619.
- (69) Huang, J. Electrochim. Acta 2018, 281, 170-188.
- (70) Sauerbrey, G. Eur. Phys. J. A 1959, 155, 206-222.
- (71) Levi, M. D.; Daikhin, L.; Aurbach, D.; Presser, V. Electrochem. Commun. 2016, 67, 16-21.
- (72) Levi, M. D.; Shpigel, N.; Sigalov, S.; Dargel, V.; Daikhin, L.; Aurbach, D. Electrochim. Acta 2017, 232, 271–284.
- (73) Shpigel, N.; Levi, M. D.; Sigalov, S.; Girshevitz, O.; Aurbach, D.; Daikhin, L.; Pikma, P.; Marandi, M.; Jänes, A.; Lust, E.; Jäckel, N.; Presser, V. Nat. Mater. 2016, 15, 570.
- (74) Dargel, V.; Jäckel, N.; Shpigel, N.; Sigalov, S.; Levi, M. D.; Daikhin, L.; Presser, V.; Aurbach, D. ACS Appl. Mater. Interfaces 2017, 9, 27664–27675.
- (75) Shpigel, N.; Lukatskaya, M. R.; Sigalov, S.; Ren, C. E.; Nayak, P.; Levi, M. D.; Daikhin, L.; Aurbach, D.; Gogotsi, Y. ACS Energy Lett. 2017, 2, 1407–1415.
- (76) Jäckel, N.; Dargel, V.; Shpigel, N.; Sigalov, S.; Levi, M. D.; Daikhin, L.; Aurbach, D.; Presser, V. J. Power Sources 2017, 371, 162–166.
- (77) Goubaa, H.; Escobar-Teran, F.; Ressam, I.; Gao, W.; El Kadib, A.; Lucas, I. T.; Raihane, M.; Lahcini, M.; Perrot, H.; Sel, O. *J. Phys. Chem.* C 2017, 121, 9370–9380.
- (78) Wen, C. J.; Boukamp, B. A.; Huggins, R. A.; Weppner, W. J. Electrochem. Soc. 1979, 126, 2258–2266.
- (79) Weppner, W.; Huggins, R. A. J. Electrochem. Soc. 1977, 124, 1569-1578.
- (80) Richard Prabakar, S. J.; Han, S. C.; Jeong, J.; Sohn, K.-S.; Pyo, M. Mater. Des. 2017, 118, 294-303.
- (81) Bard, A. J.; Fan, F. R. F.; Kwak, J.; Lev, O. Anal. Chem. 1989, 61, 132-138.
- (82) Gossage, Z. T.; Hernández-Burgos, K.; Moore, J. S.; Rodríguez-López, J. ChemElectroChem 2018, 5, 3006–3013.
- (83) Ventosa, E.; Schuhmann, W. Phys. Chem. Chem. Phys. 2015, 17, 28441–28450.
- (84) Hui, J.; Pakhira, S.; Bhargava, R.; Barton, Z. J.; Zhou, X.; Chinderle, A. J.; Mendoza-Cortes, J. L.; Rodríguez-López, J. ACS Nano 2018, 12, 2980–2990.
- (85) Zhou, X.; Gossage, Z. T.; Simpson, B. H.; Hui, J.; Barton, Z. J.; Rodríguez-López, J. ACS Nano 2016, 10, 9346–9352.
- (86) Hui, J.; Zhou, X.; Bhargava, R.; Chinderle, A.; Zhang, J.; Rodríguez-López, J. Electrochim. Acta 2016, 211, 1016–1023.
- (87) Burgess, M.; Chénard, E.; Hernández-Burgos, K.; Nagarjuna, G.; Assary, R. S.; Hui, J.; Moore, J. S.; Rodríguez-López, J. Chem. Mater. 2016, 28, 7362–7374.
- (88) Shen, M.; Qu, Z.; DesLaurier, J.; Welle, T. M.; Sweedler, J. V.; Chen, R. J. Am. Chem. Soc. 2018, 140, 7764-7768.

- (89) Lin, T.-E.; Rapino, S.; Girault, H. H.; Lesch, A. Chem. Sci. 2018, 9, 4546–4554.
- (90) Bülter, H.; Peters, F.; Schwenzel, J.; Wittstock, G. Angew. Chem., Int. Ed. 2014, 53, 10531–10535.
- (91) Bülter, H.; Sternad, M.; Santos Sardinha, E. d.; Witt, J.; Dosche, C.; Wilkening, M.; Wittstock, G. *J. Electrochem. Soc.* 2016, 163, A504—A512.
- (92) Barton, Z. J.; Rodríguez-López, J. Anal. Chem. 2017, 89, 2716-2723.
- (93) Polcari, D.; Dauphin-Ducharme, P.; Mauzeroll, J. Chem. Rev. 2016, 116, 13234-13278.
- (94) Lefrou, C.; Cornut, R. ChemPhysChem 2010, 11, 547-556.
- (95) Bülter, H.; Peters, F.; Schwenzel, J.; Wittstock, G. J. Electrochem. Soc. 2016, 163, A27-A34.
- (96) Chen, Y.; Gao, X.; Johnson, L. R.; Bruce, P. G. Nat. Commun. 2018, 9, 767.
- (97) Gossage, Z. T.; Schorr, N. B.; Hernández-Burgos, K.; Hui, J.; Simpson, B. H.; Montoto, E. C.; Rodríguez-López, J. *Langmuir* 2017, 33, 9455–9463.
- (98) Bülter, H.; Schwager, P.; Fenske, D.; Wittstock, G. *Electrochim*. *Acta* 2016, 199, 366-379.
- (99) Bülter, H.; Peters, F.; Wittstock, G. Energy Technol. 2016, 4, 1486-1494.
- (100) Zampardi, G.; Trocoli, R.; Schuhmann, W.; La Mantia, F. Phys. Chem. Chem. Phys. 2017, 19, 28381–28387.
- (101) Zampardi, G.; La Mantia, F.; Schuhmann, W. Electrochem. Commun. 2015, 58, 1-5.
- (102) Bülter, H.; Peters, F.; Schwenzel, J.; Wittstock, G. ECS Trans. 2015, 66, 69-79.
- (103) Qian, Q.; Yang, Y.; Shao, H. Phys. Chem. Chem. Phys. 2017, 19, 28772-28780.
- (104) Burgess, M.; Hernández-Burgos, K.; Cheng, K. J.; Moore, J. S.; Rodríguez-López, J. Analyst 2016, 141, 3842—3850.
- (105) Simpson, B. H.; Rodríguez-López, J. J. Am. Chem. Soc. 2015, 137, 14865-14868.
- (106) Barton, Z. J.; Hui, J.; Schorr, N. B.; Rodríguez-López, J. Electrochim. Acta 2017, 241, 98-105.
- (107) Zampardi, G.; La Mantia, F.; Schuhmann, W. RSC Adv. 2015, 5, 31166-31171.
- (108) Li, W.; Dolocan, A.; Oh, P.; Celio, H.; Park, S.; Cho, J.; Manthiram, A. Nat. Commun. 2017, 8, 14589.
- (109) Ventosa, E.; Wilde, P.; Zinn, A. H.; Trautmann, M.; Ludwig, A.; Schuhmann, W. Chem. Commun. 2016, 52, 6825–6828.
- (110) Ventosa, E.; Madej, E.; Zampardi, G.; Mei, B.; Weide, P.; Antoni, H.; La Mantia, F.; Muhler, M.; Schuhmann, W. ACS Appl. Mater. Interfaces 2017, 9, 3123-3130.
- (111) Park, J.; Kumar, V.; Wang, X.; Lee, P. S.; Kim, W. ACS Appl. Mater. Interfaces 2017, 9, 33728-33734.
- (112) Schwager, P.; Dongmo, S.; Fenske, D.; Wittstock, G. Phys. Chem. Chem. Phys. 2016, 18, 10774-10780.
- (113) Yan, R.; Ghilane, J.; Phuah, K. C.; Pham Truong, T. N.; Adams, S.; Randriamahazaka, H.; Wang, Q. J. Phys. Chem. Lett. 2018, 9, 491–496.
- (114) Barton, Z. J.; Rodríguez-López, J. Anal. Chem. 2014, 86, 10660–10667.
- (115) Barton, Z. J.; Rodríguez-López, J. Anal. Chem. 2017, 89, 2708-2715.
- (116) Schorr, N. B.; Jiang, A. G.; Rodríguez-López, J. Anal. Chem. 2018, 90, 7848-7854.
- (117) Clausmeyer, J.; Nebel, M.; Grützke, S.; Kayran, Y. U.; Schuhmann, W. ChemPlusChem 2018, 83, 414–417.
- (118) Barforoush, J. M.; McDonald, T. D.; Desai, T. A.; Widrig, D.; Bayer, C.; Brown, M. K.; Cummings, L. C.; Leonard, K. C. *Electrochim. Acta* 2016, 190, 713–719.
- (119) Kiss, A.; Nagy, G. Electroanalysis 2015, 27, 587-590.
- (120) Kuss, S.; Trinh, D.; Danis, L.; Mauzeroll, J. Anal. Chem. 2015, 87, 8096-8101.
- (121) Stephens, L. I.; Mauzeroll, J. Anal. Chem. 2018, 90, 6796-6803.
- (122) Meloni, G. N. Anal. Chem. 2017, 89, 8643-8649.

- (123) Hansma, P. K.; Drake, B.; Marti, O.; Gould, S. A.; Prater, C. B. Science 1989, 243, 641.
- (124) Chen, C.-C.; Zhou, Y.; Baker, L. A. Annu. Rev. Anal. Chem. 2012, 5, 207-228.
- (125) Page, A.; Perry, D.; Unwin, P. R. Proc. R. Soc. London, Ser. A 2017, 473, 20160889.
- (126) Ida, H.; Takahashi, Y.; Kumatani, A.; Shiku, H.; Matsue, T. Anal. Chem. 2017, 89, 6015–6020.
- (127) Sa, N.; Baker, L. A. J. Am. Chem. Soc. 2011, 133, 10398-10401.
- (128) Lipson, A. L.; Ginder, R. S.; Hersam, M. C. Adv. Mater. 2011, 23, 5613-5617.
- (129) Dorwling-Carter, L.; Aramesh, M.; Han, H.; Zambelli, T.; Momotenko, D. *Anal. Chem.* 2018, 90, 11453-11460.
- (130) Lipson, A. L.; Puntambekar, K.; Comstock, D. J.; Meng, X.; Geier, M. L.; Elam, J. W.; Hersam, M. C. *Chem. Mater.* 2014, 26, 935–940
- (131) Plett, T.; Shi, W.; Zeng, Y.; Mann, W.; Vlassiouk, I.; Baker, L. A.; Siwy, Z. S. *Nanoscale* 2015, 7, 19080–19091.
- (132) Kang, M.; Perry, D.; Bentley, C. L.; West, G.; Page, A.; Unwin, P. R. ACS Nano 2017, 11, 9525-9535.
- (133) Takahashi, Y.; Shevchuk, A. I.; Novak, P.; Murakami, Y.; Shiku, H.; Korchev, Y. E.; Matsue, T. J. Am. Chem. Soc. 2010, 132, 10118–10126.
- (134) Comstock, D. J.; Elam, J. W.; Pellin, M. J.; Hersam, M. C. Anal. Chem. 2010, 82, 1270-1276.
- (135) Takahashi, Y.; Ida, H.; Matsumae, Y.; Komaki, H.; Zhou, Y.; Kumatani, A.; Kanzaki, M.; Shiku, H.; Matsue, T. Phys. Chem. Chem. Phys. 2017, 19, 26728–26733.
- (136) Panday, N.; Qian, G.; Wang, X.; Chang, S.; Pandey, P.; He, J. ACS Nano 2016, 10, 11237-11248.
- (137) Williams, C. G.; Edwards, M. A.; Colley, A. L.; Macpherson, J. V.; Unwin, P. R. Anal. Chem. 2009, 81, 2486-2495.
- (138) Snowden, M. E.; Dayeh, M.; Payne, N. A.; Gervais, S.; Mauzeroll, J.; Schougaard, S. B. J. Power Sources 2016, 325, 682-689.
- (139) Dayeh, M.; Ghavidel, M. R. Z.; Mauzeroll, J.; Schougaard, S. B. ChemElectroChem 2018, 5, 1–8.
- (140) Takahashi, Y.; Kumatani, A.; Munakata, H.; Inomata, H.; Ito, K.; Ino, K.; Shiku, H.; Unwin, P. R.; Korchev, Y. E.; Kanamura, K.; Matsue, T. Nat. Commun. 2014, 5, 5450.
- (141) E, S. P.; Kang, M.; Wilson, P.; Meng, L.; Perry, D.; Basile, A.; Unwin, P. R. Chem. Commun. 2018, 54, 3053-3056.
- (142) Ebejer, N.; Schnippering, M.; Colburn, A. W.; Edwards, M. A.; Unwin, P. R. Anal. Chem. 2010, 82, 9141–9145.
- (143) Ebejer, N.; Güell, A. G.; Lai, S. C. S.; McKelvey, K.; Snowden, M. E.; Unwin, P. R. Annu. Rev. Anal. Chem. 2013, 6, 329–351.
- (144) Güell, A. G.; Cuharuc, A. S.; Kim, Y.-R.; Zhang, G.; Tan, S.-y.; Ebejer, N.; Unwin, P. R. ACS Nano 2015, 9, 3558–3571.
- (145) Aaronson, B. D. B.; Lai, S. C. S.; Unwin, P. R. Langmuir 2014, 30, 1915–1919.
- (146) Aaronson, B. D. B.; Byers, J. C.; Colburn, A. W.; McKelvey, K.; Unwin, P. R. Anal. Chem. 2015, 87, 4129-4133.
- (147) Momotenko, D.; Byers, J. C.; McKelvey, K.; Kang, M.; Unwin, P. R. ACS Nano 2015, 9, 8942-8952.
- (148) Wang, S.; Liu, Q.; Zhao, C.; Lv, F.; Qin, X.; Du, H.; Kang, F.; Li, B. Energy Environ. Mater. 2018, 1, 28–40.
- (149) Seidl, L.; Martens, S.; Ma, J.; Stimming, U.; Schneider, O. *Nanoscale* 2016, 8, 14004–14014.
- (150) Lu, W.; Zhang, J.; Xu, J.; Wu, X.; Chen, L. ACS Appl. Mater. Interfaces 2017, 9, 19313-19318.
- (151) Lacey, S. D.; Wan, J.; Cresce, A. v. W.; Russell, S. M.; Dai, J.; Bao, W.; Xu, K.; Hu, L. Nano Lett. 2015, 15, 1018–1024.
- (152) Han, M.; Zhu, C.; Zhao, Q.; Chen, C.; Tao, Z.; Xie, W.; Cheng, F.; Chen, J. ACS Appl. Mater. Interfaces 2017, 9, 28620-28626.
- (153) Fukutsuka, T.; Kokumai, R.; Song, H.-Y.; Takeuchi, S.; Miyazaki, K.; Abe, T. J. Electrochem. Soc. 2017, 164, A48-A53.
- (154) Lin, L.; Yang, K.; Tan, R.; Li, M.; Fu, S.; Liu, T.; Chen, H.; Pan, F. J. Mater. Chem. A 2017, 5, 19364–19370.
- (155) Huang, S.; Wang, S.; Hu, G.; Cheong, L.-Z.; Shen, C. Appl. Surf. Sci. 2018, 441, 265–271.

- (156) Li, N.-W.; Shi, Y.; Yin, Y.-X.; Zeng, X.-X.; Li, J.-Y.; Li, C.-J.; Wan, L.-J.; Wen, R.; Guo, Y.-G. Angew. Chem., Int. Ed. 2018, 57, 1505–1509. (157) Dalavi, S.; Guduru, P.; Lucht, B. L. J. Electrochem. Soc. 2012, 159, A642–A646.
- (158) Shen, C.; Wang, S.; Jin, Y.; Han, W.-Q. ACS Appl. Mater. Interfaces 2015, 7, 25441-25447.
- (159) Wang, S.; Zhang, W.; Chen, Y.; Dai, Z.; Zhao, C.; Wang, D.; Shen, C. Appl. Surf. Sci. 2017, 426, 217–223.
- (160) Haruta, M.; Kijima, Y.; Hioki, R.; Doi, T.; Inaba, M. Nanoscale 2018, 10, 17257–17264.
- (161) Shen, C.; Hu, G.; Cheong, L.-Z.; Huang, S.; Zhang, J.-G.; Wang, D. Small Methods 2018, 2, 1700298.
- (162) Han, M.; Zhu, C.; Ma, T.; Pan, Z.; Tao, Z.; Chen, J. Chem. Commun. 2018, 54, 2381-2384.
- (163) Tokranov, A.; Sheldon, B. W.; Li, C.; Minne, S.; Xiao, X. ACS Appl. Mater. Interfaces 2014, 6, 6672–6686.
- (164) Huang, S.; Cheong, L.-Z.; Wang, S.; Wang, D.; Shen, C. Appl. Surf. Sci. 2018, 452, 67-74.
- (165) Wu, J.; Yang, S.; Cai, W.; Bi, Z.; Shang, G.; Yao, J. Sci. Rep. 2017, 7, 11164.
- (166) Yang, S.; Yan, B.; Wu, J.; Lu, L.; Zeng, K. ACS Appl. Mater. Interfaces 2017, 9, 13999-14005.
- (167) Milev, A.; George, L.; Khan, S.; Selvam, P.; Kamali Kannangara, G. S. Electrochim. Acta 2016, 209, 565–573.
- (168) Park, H. S.; Jang, J. H. J. Electrochem. Sci. Technol. 2016, 7, 316—
- (169) Zampardi, G.; Klink, S.; Kuznetsov, V.; Erichsen, T.; Maljusch, A.; La Mantia, F.; Schuhmann, W.; Ventosa, E. ChemElectroChem 2015, 2, 1607–1611.
- (170) Velmurugan, J.; Agrawal, A.; An, S.; Choudhary, E.; Szalai, V. A. Anal. Chem. 2017, 89, 2687–2691.
- (171) Kranz, C.; Friedbacher, G.; Mizaikoff, B.; Lugstein, A.; Smoliner, J.; Bertagnolli, E. Anal. Chem. 2001, 73, 2491–2500.
- (172) Huang, Z.; De Wolf, P.; Poddar, R.; Li, C.; Mark, A.; Nellist, M. R.; Chen, Y.; Jiang, J.; Papastavrou, G.; Boettcher, S. W.; Xiang, C.; Brunschwig, B. S. *Microsc. Today* 2016, 24, 18–25.
- (173) Deng, Y.; Dong, S.; Li, Z.; Jiang, H.; Zhang, X.; Ji, X. Small Methods 2018, 2, 1700332.
- (174) Pérez-Villar, S.; Lanz, P.; Schneider, H.; Novák, P. Electrochim. Acta 2013, 106, 506-515.
- (175) Huth, F.; Govyadinov, A.; Amarie, S.; Nuansing, W.; Keilmann, F.; Hillenbrand, R. Nano Lett. 2012, 12, 3973–3978.
- (176) Freitas, R. O.; Deneke, C.; Maia, F. C. B.; Medeiros, H. G.; Moreno, T.; Dumas, P.; Petroff, Y.; Westfahl, H. *Opt. Express* 2018, 26, 11238–11249.
- (177) Richey, F. W.; Dyatkin, B.; Gogotsi, Y.; Elabd, Y. A. J. Am. Chem. Soc. 2013, 135, 12818-12826.
- (178) Richey, F. W.; Tran, C.; Kalra, V.; Elabd, Y. A. J. Phys. Chem. C 2014, 118, 21846-21855.
- (179) Kuwata, H.; Matsui, M.; Sonoki, H.; Manabe, Y.; Imanishi, N.; Mizuhata, M. J. Electrochem. Soc. 2018, 165, A1486–A1491.
- (180) Shi, F.; Ross, P. N.; Somorjai, G. A.; Komvopoulos, K. J. Phys. Chem. C 2017, 121, 14476–14483.
- (181) Vivek, J. P.; Berry, N. G.; Zou, J.; Nichols, R. J.; Hardwick, L. J. J. Phys. Chem. C 2017, 121, 19657–19667.
- (182) Mudunkotuwa, I. A.; Minshid, A. A.; Grassian, V. H. Analyst 2014, 139, 870-881.
- (183) Haregewoin, A. M.; Shie, T.-D.; Lin, S. D.; Hwang, B.-J.; Wang, F.-M. ECS Trans. 2013, 53, 23–32.
- (184) Yohannes, Y. B.; Lin, S. D.; Wu, N.-L. J. Electrochem. Soc. 2017, 164, A3641-A3648.
- (185) Son, I. H.; Park, J. H.; Kwon, S.; Mun, J.; Choi, J. W. Chem. Mater. 2015, 27, 7370-7379.
- (186) Teshager, M. A.; Hwang, B.-J.; Chern, Y.-T.; Lin, S. D. ChemElectroChem 2017, 4, 201–208.
- (187) Teshager, M. A.; Lin, S. D.; Hwang, B.-J.; Wang, F.-M.; Hy, S.; Haregewoin, A. M. ChemElectroChem 2016, 3, 337–345.
- (188) Vivek, J. P.; Berry, N.; Papageorgiou, G.; Nichols, R. J.; Hardwick, L. J. J. Am. Chem. Soc. 2016, 138, 3745-3751.

- (189) Osawa, M. Bull. Chem. Soc. Jpn. 1997, 70, 2861-2880.
- (190) Mozhzhukhina, N.; Tesio, A. Y.; De Leo, L. P. M.; Calvo, E. J. J. Electrochem. Soc. 2017, 164, A518-A523.
- (191) Kuwata, H.; Matsui, M.; Imanishi, N. J. Electrochem. Soc. 2017, 164. A3229-A3236.
- (192) Lucas, I. T.; McLeod, A. S.; Syzdek, J. S.; Middlemiss, D. S.; Grey, C. P.; Basov, D. N.; Kostecki, R. *Nano Lett.* 2015, 15, 1–7.
- (193) Galloway, T. A.; Hardwick, L. J. J. Phys. Chem. Lett. 2016, 7, 2119-2124.
- (194) Galloway, T. A.; Cabo-Fernandez, L.; Aldous, I. M.; Braga, F.; Hardwick, L. J. Faraday Discuss. 2017, 205, 469–490.
- (195) Kumar, N.; Su, W.; Veselý, M.; Weckhuysen, B. M.; Pollard, A. J.; Wain, A. J. Nanoscale 2018, 10, 1815-1824.
- (196) Martín Sabanés, N.; Driessen, L. M. A.; Domke, K. F. Anal. Chem. 2016, 88, 7108-7114.
- (197) Olson, J. Z.; Johansson, P. K.; Castner, D. G.; Schlenker, C. W. Chem. Mater. 2018, 30, 1239-1248.
- (198) Peng, Q.; Liu, H.; Ye, S. J. Electroanal. Chem. 2017, 800, 134-
- (199) Maruyama, S.; Fukutsuka, T.; Miyazaki, K.; Abe, Y.; Yoshizawa, N.; Abe, T. *J. Mater. Chem. A* 2018, 6, 1128–1137.
- (200) Wu, H.-L.; Shin, M.; Liu, Y.-M.; See, K. A.; Gewirth, A. A. Nano Energy 2017, 32, 50-58.
- (201) Chao, D.; Liang, P.; Chen, Z.; Bai, L.; Shen, H.; Liu, X.; Xia, X.; Zhao, Y.; Savilov, S. V.; Lin, J.; Shen, Z. X. ACS Nano 2016, 10, 10211–10219.
- (202) Childress, A. S.; Parajuli, P.; Zhu, J.; Podila, R.; Rao, A. M. Nano Energy 2017, 39, 69-76.
- (203) Sang, L.; Haasch, R. T.; Gewirth, A. A.; Nuzzo, R. G. Chem. Mater. 2017, 29, 3029-3037.
- (204) Kurouski, D.; Mattei, M.; Van Duyne, R. P. *Nano Lett.* 2015, 15, 7956–7962.
- (205) Hy, S.; Felix, F.; Rick, J.; Su, W.-N.; Hwang, B. J. J. Am. Chem. Soc. 2014, 136, 999-1007.
- (206) Radjenovic, P. M.; Hardwick, L. J. Faraday Discuss. 2018, 206, 379–392.
- (207) Aldous, I. M.; Hardwick, L. J. Angew. Chem. 2016, 128, 8394—8397.
- (208) Johnson, L.; Li, C.; Liu, Z.; Chen, Y.; Freunberger, S. A.; Ashok, P. C.; Praveen, B. B.; Dholakia, K.; Tarascon, J.-M.; Bruce, P. G. *Nat. Chem.* 2014, *6*, 1091.
- (209) Cabo-Fernandez, L.; Bresser, D.; Braga, F.; Passerini, S.; Hardwick, L. J. *In Situ* Electrochemical SHINERS Investigation of SEI Composition on Carbon-Coated Zn_{0.9}Fe_{0.1}O Anode for Lithium-Ion Batteries. *Batteries & Supercaps* 2018, DOI: 10.1002/batt.201800063.
- (210) Mattei, M.; Kang, G.; Goubert, G.; Chulhai, D. V.; Schatz, G. C.; Jensen, L.; Van Duyne, R. P. *Nano Lett.* 2017, *17*, 590–596.
- (211) Touzalin, T.; Joiret, S.; Maisonhaute, E.; Lucas, I. T. Anal. Chem. 2017, 89, 8974–8980.
- (212) Su, W.; Kumar, N.; Krayev, A.; Chaigneau, M. Nat. Commun. 2018, 9, 2891.
- (213) Wang, H.-F.; Gan, W.; Lu, R.; Rao, Y.; Wu, B.-H. Int. Rev. Phys. Chem. 2005, 24, 191–256.
- (214) Yan, E. C. Y.; Fu, L.; Wang, Z.; Liu, W. Chem. Rev. 2014, 114, 8471–8498.
- (215) Yu, L.; Liu, H.; Wang, Y.; Kuwata, N.; Osawa, M.; Kawamura, J.; Ye, S. Angew. Chem. 2013, 125, 5865–5868.
- (216) Nicolau, B. G.; García-Rey, N.; Dryzhakov, B.; Dlott, D. D. J. Phys. Chem. C 2015, 119, 10227-10233.
- (217) Horowitz, Y.; Han, H.-L.; Ross, P. N.; Somorjai, G. A. J. Am. Chem. Soc. 2016, 138, 726-729.
- (218) Horowitz, Y.; Han, H.-L.; Ralston, W. T.; de Araujo, J. R.; Kreidler, E.; Brooks, C.; Somorjai, G. A. Adv. Energy Mater. 2017, 7, 1602060.
- (219) Hernandez, M.; Chinwangso, P.; Cimatu, K.; Srisombat, L.-o.; Lee, T. R.; Baldelli, S. *J. Phys. Chem. C* 2011, *115*, 4688–4695.
- (220) Cimatu, K.; Baldelli, S. J. Am. Chem. Soc. 2008, 130, 8030-8037.
- (221) Bressler, C.; Chergui, M. Chem. Rev. 2004, 104, 1781-1812.

- (222) Takamatsu, D.; Koyama, Y.; Orikasa, Y.; Mori, S.; Nakatsutsumi, T.; Hirano, T.; Tanida, H.; Arai, H.; Uchimoto, Y.; Ogumi, Z. Angew. Chem., Int. Ed. 2012, 51, 11597—11601.
- (223) Zhang, L.; Ling, M.; Feng, J.; Mai, L.; Liu, G.; Guo, J. Energy Storage Mater. 2018, 11, 24-29.
- (224) Miller, E. C.; Kasse, R. M.; Heath, K. N.; Perdue, B. R.; Toney, M. F. J. Electrochem. Soc. 2018, 165, A6043-A6050.
- (225) Tang, C.-Y.; Feng, L.; Haasch, R. T.; Dillon, S. J. Electrochim. Acta 2018, 277, 197-204.
- (226) Chen, X.; Vörös, M.; Garcia, J. C.; Fister, T. T.; Buchholz, D. B.; Franklin, J.; Du, Y.; Droubay, T. C.; Feng, Z.; Iddir, H.; Curtiss, L. A.; Bedzyk, M. J.; Fenter, P. ACS Appl. Energy Mater. 2018, 1, 2526–2535.
- (227) Kawaura, H.; Harada, M.; Kondo, Y.; Kondo, H.; Suganuma, Y.; Takahashi, N.; Sugiyama, J.; Seno, Y.; Yamada, N. L. ACS Appl. Mater. Interfaces 2016, 8, 9540–9544.
- (228) Steinhauer, M.; Stich, M.; Kurniawan, M.; Seidlhofer, B.-K.; Trapp, M.; Bund, A.; Wagner, N.; Friedrich, K. A. ACS Appl. Mater. Interfaces 2017, 9, 35794–35801.
- (229) Ding, Y.; Li, Z.-F.; Timofeeva, E. V.; Segre, C. U. Adv. Energy Mater. 2018, 8, 1702134.
- (230) Yu, S.-H.; Jin, A.; Huang, X.; Yang, Y.; Huang, R.; Brock, J. D.; Sung, Y.-E.; Abruña, H. D. RSC Adv. 2018, 8, 23847–23853.
- (231) Lowe, M. A.; Gao, J.; Abruña, H. D. J. Mater. Chem. A 2013, 1, 2094-2103.
- (232) Wandt, J.; Freiberg, A.; Thomas, R.; Gorlin, Y.; Siebel, A.; Jung, R.; Gasteiger, H. A.; Tromp, M. J. Mater. Chem. A 2016, 4, 18300–18305.
- (233) Hong, L.; Li, L.; Chen-Wiegart, Y.-K.; Wang, J.; Xiang, K.; Gan, L.; Li, W.; Meng, F.; Wang, F.; Wang, J.; Chiang, Y.-M.; Jin, S.; Tang, M. Nat. Commun. 2017, 8, 1194.
- (234) Wang, J.; Karen Chen-Wiegart, Y.-c.; Eng, C.; Shen, Q.; Wang, J. Nat. Commun. 2016, 7, 12372.
- (235) Takamatsu, D.; Orikasa, Y.; Mori, S.; Nakatsutsumi, T.; Yamamoto, K.; Koyama, Y.; Minato, T.; Hirano, T.; Tanida, H.; Arai, H.; Uchimoto, Y.; Ogumi, Z. *J. Phys. Chem. C* 2015, *119*, 9791–9797.
- (236) Takamatsu, D.; Nakatsutsumi, T.; Mori, S.; Orikasa, Y.; Mogi, M.; Yamashige, H.; Sato, K.; Fujimoto, T.; Takanashi, Y.; Murayama, H.; Oishi, M.; Tanida, H.; Uruga, T.; Arai, H.; Uchimoto, Y.; Ogumi, Z. J. Phys. Chem. Lett. 2011, 2, 2511–2514.
- (237) Takamatsu, D.; Mori, S.; Orikasa, Y.; Nakatsutsumi, T.; Koyama, Y.; Tanida, H.; Arai, H.; Uchimoto, Y.; Ogumi, Z. J. Electrochem. Soc. 2013, 160, A3054—A3060.
- (238) Yu, S.-H.; Huang, X.; Schwarz, K.; Huang, R.; Arias, T. A.; Brock, J. D.; Abruña, H. D. Energy Environ. Sci. 2018, 11, 202–210.
- (239) Cheng, J.-H.; Assegie, A. A.; Huang, C.-J.; Lin, M.-H.; Tripathi, A. M.; Wang, C.-C.; Tang, M.-T.; Song, Y.-F.; Su, W.-N.; Hwang, B. J. J. Phys. Chem. C 2017, 121, 7761–7766.
- (240) Gauthier, M.; Karayaylali, P.; Giordano, L.; Feng, S.; Lux, S. F.; Maglia, F.; Lamp, P.; Shao-Horn, Y. J. Electrochem. Soc. 2018, 165, A1377—A1387.
- (241) Wood, K. N.; Steirer, K. X.; Hafner, S. E.; Ban, C.; Santhanagopalan, S.; Lee, S.-H.; Teeter, G. Nat. Commun. 2018, 9, 2490.
- (242) Koerver, R.; Walther, F.; Aygün, I.; Sann, J.; Dietrich, C.; Zeier, W. G.; Janek, J. J. Mater. Chem. A 2017, 5, 22750–22760.
- (243) Maibach, J.; Xu, C.; Eriksson, S. K.; Åhlund, J.; Gustafsson, T.; Siegbahn, H.; Rensmo, H.; Edström, K.; Hahlin, M. Rev. Sci. Instrum. 2015, 86, 044101.
- (244) Tang, C.-Y.; Haasch, R. T.; Dillon, S. J. Chem. Commun. 2016, 52, 13257-13260.
- (245) Wong, R. A.; Yokota, Y.; Wakisaka, M.; Inukai, J.; Kim, Y. J. Am. Chem. Soc. 2018, 140, 13672-13679.
- (246) Evmenenko, G.; Fister, T. T.; Buchholz, D. B.; Li, Q.; Chen, K.-S.; Wu, J.; Dravid, V. P.; Hersam, M. C.; Fenter, P.; Bedzyk, M. ACS Appl. Mater. Interfaces 2016, 8, 19979–19986.
- (247) Plaza, M.; Huang, X.; Ko, J. Y. P.; Shen, M.; Simpson, B. H.; Rodríguez-López, J.; Ritzert, N. L.; Letchworth-Weaver, K.; Gunceler, D.; Schlom, D. G.; Arias, T. A.; Brock, J. D.; Abruña, H. D. J. Am. Chem. Soc. 2016, 138, 7816–7819.

(248) Jerliu, B.; Hüger, E.; Dörrer, L.; Seidlhofer, B. K.; Steitz, R.; Horisberger, M.; Schmidt, H. Phys. Chem. Chem. Phys. 2018, 20, 23480–23491.

- (249) Avdeev, M. V.; Rulev, A. A.; Bodnarchuk, V. I.; Ushakova, E. E.; Petrenko, V. I.; Gapon, I. V.; Tomchuk, O. V.; Matveev, V. A.; Pleshanov, N. K.; Kataev, E. Y.; Yashina, L. V.; Itkis, D. M. Appl. Surf. Sci. 2017, 424, 378–382.
- (250) Zeng, Z.; Zheng, W.; Zheng, H. Acc. Chem. Res. 2017, 50, 1808—1817.
- (251) Liu, Q.; Geng, L.; Yang, T.; Tang, Y.; Jia, P.; Li, Y.; Li, H.; Shen, T.; Zhang, L.; Huang, J. *In situ* Imaging Electrocatalysis in a Na-O₂ Battery with Au-Coated MnO₂ Nanowires Air Cathode. *Energy Storage Mater.* 2018, in press; DOI: 10.1016/j.ensm.2018.08.026
- (252) Holtz, M. E.; Yu, Y.; Gunceler, D.; Gao, J.; Sundararaman, R.; Schwarz, K. A.; Arias, T. A.; Abruña, H. D.; Muller, D. A. *Nano Lett.* 2014, 14, 1453–1459.
- (253) Xie, Z.-H.; Jiang, Z.; Zhang, X. J. Electrochem. Soc. 2017, 164, A2110-A2123.
- (254) Lutz, L.; Dachraoui, W.; Demortière, A.; Johnson, L. R.; Bruce, P. G.; Grimaud, A.; Tarascon, J.-M. *Nano Lett.* 2018, 18, 1280–1289. (255) Cheong, J. Y.; Chang, J. H.; Seo, H. K.; Yuk, J. M.; Shin, J. W.; Lee, J. Y.; Kim, I.-D. *Nano Energy* 2016, 25, 154–160.
- (256) Yuk, J. M.; Park, J.; Ercius, P.; Kim, K.; Hellebusch, D. J.; Crommie, M. F.; Lee, J. Y.; Zettl, A.; Alivisatos, A. P. Science 2012, 336, 61
- (257) Yuk, J. M.; Seo, H. K.; Choi, J. W.; Lee, J. Y. ACS Nano 2014, 8, 7478-7485.
- (258) Harrison, K. L.; Zavadil, K. R.; Hahn, N. T.; Meng, X.; Elam, J. W.; Leenheer, A.; Zhang, J.-G.; Jungjohann, K. L. ACS Nano 2017, 11, 11194–11205.
- (259) Mehdi, B. L.; Stevens, A.; Qian, J.; Park, C.; Xu, W.; Henderson, W. A.; Zhang, J.-G.; Mueller, K. T.; Browning, N. D. Sci. Rep. 2016, 6, 34267.
- (260) Rehn, S. M.; Jones, M. R. ACS Energy Lett. 2018, 3, 1269–1278. (261) Zhang, X.; Wang, X.-G.; Xie, Z.; Zhou, Z. Green Energy & Environment 2016, 1, 4–17.
- (262) Li, Y.; Lu, J. ACS Energy Lett. 2017, 2, 1370-1377.
- (263) Montoto, E. C.; Cao, Y.; Hernández-Burgos, K.; Sevov, C. S.; Braten, M. N.; Helms, B. A.; Moore, J. S.; Rodríguez-López, J. *Macromolecules* 2018, *51*, 3539–3546.
- (264) Burgess, M.; Hernández-Burgos, K.; Schuh, J. K.; Davila, J.; Montoto, E. C.; Ewoldt, R. H.; Rodríguez-López, J. J. Am. Chem. Soc. 2018, 140, 2093–2104.
- (265) Montoto, E. C.; Nagarjuna, G.; Hui, J.; Burgess, M.; Sekerak, N. M.; Hernández-Burgos, K.; Wei, T.-S.; Kneer, M.; Grolman, J.; Cheng, K. J.; Lewis, J. A.; Moore, J. S.; Rodríguez-López, J. *J. Am. Chem. Soc.* 2016, 138, 13230–13237.
- (266) Burgess, M.; Hernández-Burgos, K.; Simpson, B. H.; Lichtenstein, T.; Avetian, S.; Nagarjuna, G.; Cheng, K. J.; Moore, J. S.; Rodríguez-López, J. J. Electrochem. Soc. 2016, 163, H3006—H3013.
- (267) Nagarjuna, G.; Hui, J.; Cheng, K. J.; Lichtenstein, T.; Shen, M.; Moore, J. S.; Rodríguez-López, J. J. Am. Chem. Soc. 2014, 136, 16309—16316.
- (268) Gossage, Z. T.; Simpson, B. H.; Schorr, N. B.; Rodríguez-López, J. Anal. Chem. 2016, 88, 9897—9901.